REPORT DOCUMENTATION PAGE

1. REPORT DATE *(DD-MM-YYYY)*	2. REPORT TYPE	3. DATES COVERED *(From - To)*

4. TITLE AND SUBTITLE

5a. CONTRACT NUMBER

5b. GRANT NUMBER

5c. PROGRAM ELEMENT NUMBER

6. AUTHOR(S)

5d. PROJECT NUMBER

5e. TASK NUMBER

5f. WORK UNIT NUMBER

7. PERFORMING ORGANIZATION NAME(S) AND ADDRESS(ES)

8. PERFORMING ORGANIZATION REPORT NUMBER

9. SPONSORING/MONITORING AGENCY NAME(S) AND ADDRESS(ES)

10. SPONSOR/MONITOR'S ACRONYM(S)

11. SPONSOR/MONITOR'S REPORT NUMBER(S)

12. DISTRIBUTION/AVAILABILITY STATEMENT

13. SUPPLEMENTARY NOTES

14. ABSTRACT

15. SUBJECT TERMS

16. SECURITY CLASSIFICATION OF:			17. LIMITATION OF ABSTRACT	18. NUMBER OF PAGES	19a. NAME OF RESPONSIBLE PERSON
a. REPORT	b. ABSTRACT	c. THIS PAGE			
					19b. TELEPHONE NUMBER *(Include area code)*

NOZZLE MODIFICATIONS FOR HIGH-REYNOLDS-NUMBER QUIET FLOW

IN THE BOEING/AFOSR MACH-6 QUIET TUNNEL

A Thesis

Submitted to the Faculty

of

Purdue University

by

Thomas J. Juliano

In Partial Fulfillment of the

Requirements for the Degree

of

Master of Science in Aeronautics and Astronautics

December 2006

Purdue University

West Lafayette, Indiana

To Grandpa Lou,

from whom I inherited the enjoyment of working with my hands as well as my head.

ACKNOWLEDGMENTS

I would like to thank my advisor, Professor Steven P. Schneider, for managing the Boeing/AFOSR Mach-6 Quiet Tunnel and giving me the opportunity to work on it. The guidance and suggestions offered by my committee members, Professors Steven Collicott and Stephen Heister, are also appreciated.

I would like to thank the ASL shop, Madeleine Chadwell, Jerry Hahn, Robin Snodgrass, and Jim Younts, for their excellent craftsmanship and valuable advice. I would also like to thank Nick, Eddie, and company at Optek for their work on polishing the nozzle.

I also thank the other members of Team Schneider: Shann Rufer, Craig Skoch, Erick Swanson, Tyler Robarge, Matt Borg, and Mikey Hannon. It is impossible to imagine the last two years without their assistance and camaraderie.

Finally, I would like to credit the support offered by my family.

TABLE OF CONTENTS

LIST OF TABLES

LIST OF FIGURES

SYMBOLS

A	cross-sectional area
a	Kulite calibration constant
b	Kulite calibration constant
c_p	specific heat capacity at constant pressure
M	Mach number
p	pressure
p_t	driver tube pressure (measured at contraction entrance)
R	correlation coefficient
Re	Reynolds number
Re_k	Reynolds number based on peak-to-valley defect height and conditions in the smooth-wall laminar boundary layer at the roughness height
T	Temperature
t	time
y	radial location ($y = 0$ along centerline)
z	axial location ($z = 0$ at throat and 2.590 m at end of Section 8)
β	shock angle
γ	ratio of specific heats ($\gamma = 1.4$ used for air)

Superscripts

$*$	sonic point
$\sim$	root-mean-square (rms)
$-$	mean

Subscripts

0	total (stagnation) value
1	pre-shock value
2	post-shock value

Acronyms

ASL	Aerospace Sciences Laboratory
BAM6QT	Boeing/AFOSR Mach-6 Quiet Tunnel
CFD	Computational Fluid Dynamics
MAWP	Maximum Allowable Working Pressure

ABSTRACT

Juliano, Thomas J. M.S.A.A., Purdue University, December, 2006. Nozzle Modifications for High-Reynolds-Number Quiet Flow in the Boeing/AFOSR Mach-6 Quiet Tunnel.   Major Professor: Steven P. Schneider.

The Boeing/AFOSR Mach-6 Quiet Tunnel was designed to have laminar nozzle-wall boundary layers and therefore low noise levels for stagnation pressures (p_t) up to 150 psia. From its initial operation in 2001 until March 2005, the tunnel only exhibited low noise levels for p_t less than 8 psia. A surrogate aluminum nozzle was fabricated to replace 30 in. of the original electroformed nickel and steel nozzle, starting at the throat region. Improving the surrogate nozzle's polish and other modifications improved its maximum quiet pressure from 20 psia to as high as 130 psia, though not reliably. Quiet flow is regularly achieved for p_t less than 60–90 psia. A flaw in the electroformed nozzle bleed lip inner contour was identified as the probable cause of early transition on the electroform. Computations made at Rutgers University predict a separation bubble on the bleed lip that might well trip the nozzle-wall boundary-layer. The bleed-lip contour was remachined and the flaw was eliminated. As of August 2006, the electroformed nozzle exhibited performance similar to the surrogate. Measurements in the downstream half of the nozzle found no quiet pressure dependence on axial location, suggesting that bypass transition near the bleed lip is still responsible for the limited performance.

1. Introduction

1.1 Laminar-to-Turbulent Transition and Quiet Flow

Fluid flow in a boundary layer can exist in two regimes, laminar and turbulent, sometimes separated by a transitional phase. In natural transition, disturbances in the laminar flow, such as free-stream turbulence, free-stream vorticity disturbances, or surface roughness, are amplified through various instabilities and lead to transition to turbulent flow [1]. Larger initial disturbances will bypass the linear growth mechanisms and lead directly to turbulent flow. This process is not well understood and the prediction of bypass transition is therefore difficult.

The streamlines of particles in a laminar boundary layer are smoother and straighter than those in turbulent flow and result in less friction and heat flux at the wall [2]. The prediction and control of transition is an important factor in the design of hypersonic vehicles due to its effect on surface heating, skin friction, separation, aero-optical distortion, and other boundary-layer properties [3]. This issue is especially pressing at hypersonic velocities, Mach number > 5, due to the high energies and heating involved. Aeroheating can often be predicted accurately for both laminar and turbulent flow. The largest source of uncertainty in calculating heat flux is then the transition location, as illustrated in Figure 1.1 [4]. Reentry-heating flight data and a computational prediction are plotted as a function of distance along the body. The transition location for the computational prediction was chosen to match the flight data. The laminar and turbulent heating levels match the predicted level fairly well, but the uncertainty in transition location can cause large errors.

Many factors influence transition, including Reynolds number, surface roughness, and atmospheric conditions such as free stream noise level [5], [1]. The noise level of a flow can be defined as the ratio of root-mean-square (rms) pitot stagnation
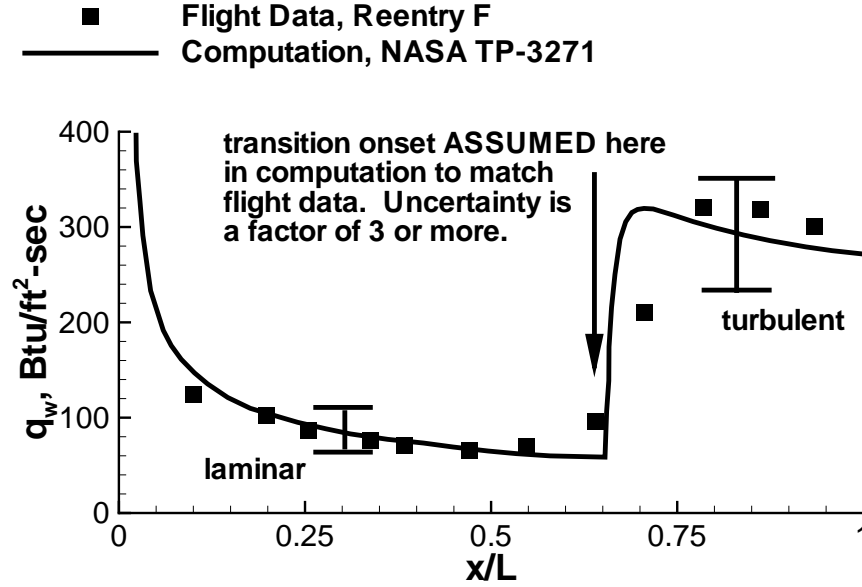
Figure 1.1: Computational & experimental heat flux (Ref. [4])

pressure to mean pitot stagnation pressure, $\tilde{p}/\bar{p}$. Atmospheric levels are typically $< 0.05\%$ [6]. Such low levels are regarded as "quiet". Accurate wind tunnel testing requires matching as many flight parameters as possible, but achieving this low noise level in a wind tunnel has been particularly difficult [7]. Conventional tunnels have noise levels of 1–3%. Thus, quiet wind tunnels are an important tool for the investigation of hypersonic transition. For instance, linear instability theory predicts a smaller transition Reynolds number for a 5° half-angle cone than for a flat plate. Wind tunnel testing in a conventional (noisy) tunnel yielded the opposite conclusion. The theory was not verified until quiet tunnel results were available [8].

Like other fluid mechanics problems, transition is studied by a combined approach of theoretical analysis, computational fluid dynamics (CFD), wind tunnel testing, and flight experimentation. Theoretical analysis is limited by the significant complexity of the problem. Any useful results are limited to specific cases that rely on several assumptions. CFD is a powerful and improving tool, but it requires careful selection of necessary approximations and substantial experimentation to verify its

results. Wind tunnels are restricted to matching only some subset of flight parameters, so they cannot stand by themselves as a design tool. Actual flight testing is the most accurate means of studying transition, but it is also the most expensive. It has several other drawbacks, including limited instrumentation and difficulty controlling angle of attack [9].

The primary reason for the difference in noise levels between conventional and quiet tunnels is that conventional tunnels have turbulent boundary layers whereas quiet tunnels have laminar boundary layers [10] – [11]. Turbulent boundary layers produce unsteady Mach waves that cause fluctuations in the pressure downstream in the test section [4]. The control of transition on the nozzle walls is a problem that needs to be overcome in order to study transition on the test articles.

Figure 1.2 is a shadowgraph of a 5° sharp cone at Mach 4.31 that illustrates many transition-related phenomena [4]. The cone is at approximately zero angle of attack in air with a unit Reynolds number of $2.66 \cdot 10^6$/inch. This image was obtained in the Naval Ordnance Lab ballistics range. The upper surface of the cone is mostly laminar with two turbulent spots. An oblique shock emanates from each of these spots. The lower surface is fully turbulent. The noise radiated into the flow by the turbulent boundary layer is visible as diagonal striations not present near the laminar boundary layer on the upper surface. Similar flow behavior occurs above the surface of a wind tunnel nozzle.

Transition occurs at a critical Reynolds number if other flow parameters (geometry, surface roughness, etc.) are constant. If the Reynolds number of a flow is less than $Re_{critical}$, the boundary layer is laminar and if it is greater, it is transitional or turbulent. In supersonic wind tunnels, the free-stream Reynolds number is controlled by changing the stagnation pressure (and thereby density) upstream of the throat. Increasing the maximum stagnation pressure at which a tunnel runs quietly allows one to simulate a wider range of flight conditions. The goal of the project is not only to obtain quiet flow, but to do so at as high a stagnation pressure as possible.
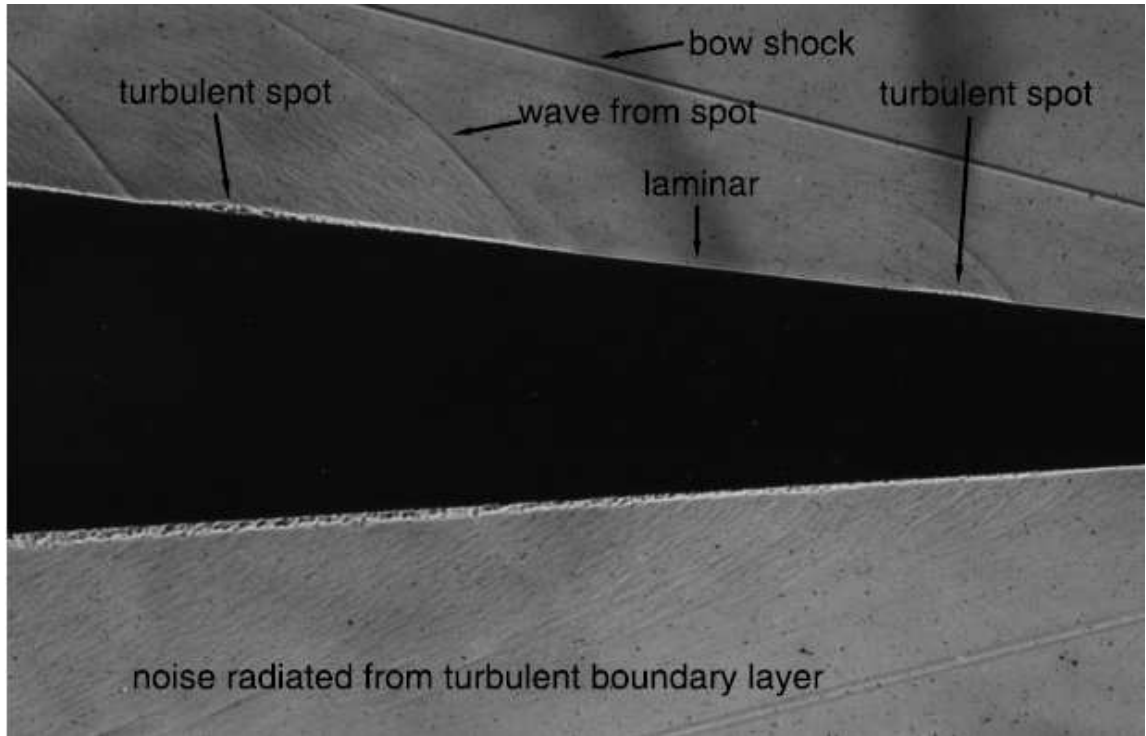
Figure 1.2: Shadowgraph of sharp cone at $M = 4.31$ (Ref. [4])

1.2 History of Quiet Tunnel Design

Quiet tunnel design was pioneered by Ivan Beckwith and others at the Gas Dynamics Section at NASA Langley in the early 1970's [6, 10, 12–18]. Conventional tunnels had demonstrated quiet performance in the past, but only at low Reynolds numbers. The Langley tunnels employed many special features. A suction slot was placed just upstream of the throat in order to remove the boundary layer there, including the Görtler vortices due to a boundary layer instability caused by the concave contraction walls. Low-noise piping and quiet valves fed a large settling chamber. Significant effort was spent testing a sound shield that was placed in the test section to muffle any noise radiated from the nozzle walls [6]. This solution was ineffective and discarded. A series of meshes and screens was placed in the set-

tling chamber to attenuate disturbances from the air supply piping [13]. Originally, a rapid-expansion, two-dimensional nozzle was used [14], but it was replaced by a long-axisymmetric Mach 3.5 nozzle with a long, straight-walled section to delay the onset of Görtler vortices. Beckwith et al. concluded that a roughness criterion of $Re_k < 12$ was required to prevent roughness-induced boundary layer transition [15].

1.3   The Boeing/AFOSR Mach-6 Quiet Tunnel

Design of the Boeing/AFOSR Mach-6 Quiet Tunnel (BAM6QT) began in 1996. From the outset, the tunnel had two goals: run with a low noise level, and do so affordably. To achieve the first goal, many of the characteristics of the Langley quiet tunnels were employed. For example, the BAM6QT incorporates boundary layer suction before the throat and the nozzle features a long, radial section to delay the onset of Görtler vortices [19]. The first 0.76 m of the nozzle features an electroformed nickel finish, which has no seams and can be highly polished with minimal roughness and waviness [20].

In order to have a low operating cost, a Ludwieg tube design was chosen over the blowdown configuration. A Ludwieg tube is a pipe with a converging/diverging (de Laval) nozzle on the end. The drawback of the Ludwieg tube is the limited run time. For the BAM6QT, the run time is about 8 seconds, compared to up to an hour for the tunnels at NASA Langley [18]. However, the advances made in data acquisition technology make it possible to gather a considerable amount of data in those 8 seconds. Whereas the Langley facility employs many technicians to maintain and operate the tunnel, the BAM6QT can be run by just one student. Another advantage of the Ludwieg-tube configuration is simplified plumbing. The entire driver tube serves as a settling chamber. The added complexity due to the various baffles and screens in a blowdown tunnel's settling chamber is unnecessary because a simple valve isolates the driver tube from the air compressor.

The BAM6QT was first run in 2001. Initially, the quiet performance was much less than hoped. Though designed to run quietly for stagnation pressures up to 150 psia, the tunnel was quiet only for $p_t < 8$ psia [21] – [22]. Several potential explanations for the low maximum quiet pressure were posed [23]. Their solutions were tested from 2001 to 2005 [24] – [28]. Alternative bleed-slot inserts were tested to determine if there was a problem with the bleed-slot flow. Vibration of the bleed lip was considered, but is unlikely to cause a problem because the frequency would be much less than that required to affect the flow. An aft-facing step at the end of the electroformed portion of the nozzle was removed. The sections of the nozzle after the electroform (Sections 5 through 7) (see Figure 1.3), which were originally just a machined finish, were polished. Leak tests were performed on the driver tube, contraction, and nozzle to detect any jets that might disrupt the boundary layer. Runs with and without the sting mount and various models were made to determine whether nozzle-wall boundary-layer separation was occurring and feeding forward. Bleed air was plumbed directly into the vacuum tank, rather than into the diffuser, to assess the effect of separation due to the incoming jets. The noise levels and temperature distribution in the contraction were measured. Heater settings were optimized and insulation was applied in order to reduce temperature fluctuations. Thermocouples were attached to the outside of the nozzle to verify that the temperature profile corresponds to that assumed in the design. A valve was added at the upstream end of the driver tube to prevent a jet of air into it. Longer settling times were tested. None of these efforts had a major impact.

In late 2002, a small bump was detected in the throat region. It was not measured until 2005 for fear of damaging the delicate polish. A surrogate nozzle was machined from aluminum and tested beginning in February 2005. This nozzle bleed lip did not have the same imperfection. This change is the first one to have a significant improvement on the quiet pressure. Between June 2005 and July 2006 numerous iterations of nozzle modifications were tested to quantify their effect on the tunnel's maximum quiet pressure.
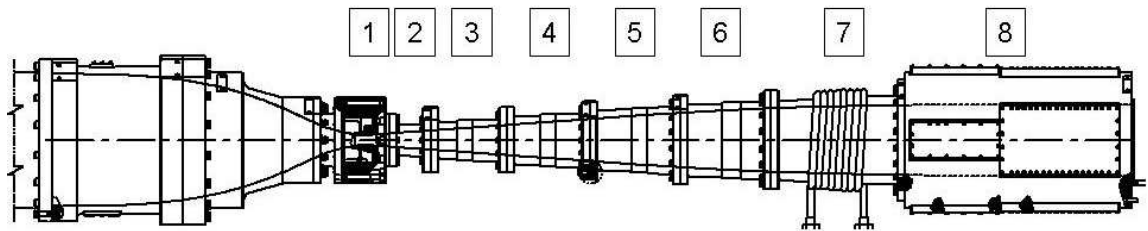
Figure 1.3: Schematic of BAM6QT nozzle with numbered sections

2. Apparatus

2.1 BAM6QT

All tests were performed in the Boeing/AFOSR Mach-6 Quiet Tunnel at the Aerospace Sciences Laboratory at Purdue University (Figure 2.1). The difference in tunnel configuration from previous work was the use of the aluminum surrogate nozzle throat instead of the electroformed nickel and steel original.

All Clean Stainless Steel from Second-Throat Section Upstream
Unique Low-Noise Flow due to Laminar Nozzle-Wall Boundary Layer
(Slow) Gate Valve

17.5-in. Driver Tube, 122.5-ft. long

Bleed-Slot Suction Plumbed Both Through Fast Valve to Tank and to Diffuser

9.5-in. Nozzle

4000 Cubic Ft. Vacuum Tank

Max. 300 psig (21.7 bar,abs.) and 392F (200C). One 10-s. run per hour. About $10/run operating cost.

Contraction   Windows

Fixed Sting Support

Diffuser

(Double) Burst Diaphragm

Sliding Sleeve

Figure 2.1: Schematic of the BAM6QT

Most of the length of the BAM6QT is the 122.5-ft-long, 18-in.-diameter driver tube (Figure 2.2). There is a solenoid-actuated valve at the upstream end of the driver tube that connects to the compressed air system. For pressures up to about 145 psia, the building's main compressed air supply is used. For pressures up to 300 psia, a boost pump has been installed. In both cases, the air is thoroughly dried and filtered. The dew point, which typically ranges from < -8 °C in the humid summer to < -30 °C during the winter, is monitored by a Panametrics Moisture Target

Series-5 dew point meter. Air entering the driver tube and the driver tube itself are heated to about 160 ℃ to avoid nitrogen liquefaction in the nozzle. Fiberglass insulation covers the driver tube. A 6-volt electric potential across the tube draws approximately 2000 amps of current to maintain the driver-tube temperature.

Figure 2.2: BAM6QT driver tube

The downstream end of the driver tube connects to the contraction, where the 18 in. diameter is faired smoothly to 1.57 in. Three band heaters are attached to the contraction to maintain the elevated temperature. The diverging portion of the nozzle (Figures 2.3 and 2.4) attaches to the downstream end of the contraction. It is constructed in eight sections (Figure 1.3). The original nozzle is 15-5 PH stainless steel, though Sections 1 through 4 have an inner electroformed layer of nickel. The surrogate nozzle is an aluminum replacement for the first four sections, the first 30.2650 in. (0.769 m) past the throat; the further-downstream sections are unchanged. The bleed lip extends forward into the end of the contraction, leaving a 0.058 in. annular gap. The boundary layer that had been building along the contraction wall is sucked away through this gap and a set of eight bleed tubes (Figure 2.5) in order to allow a new, laminar boundary layer develop on the nozzle walls. The nozzle has a 1.236 in. diameter at the throat, its narrowest point (Figure 2.6). The flow expands over the nozzle's 102 in. length to a final diameter of 9.526 in. This area expansion ratio sets the Mach number in the test section to about 6, depending on the boundary layer thickness (see section 4.4). This tunnel does not have a

dedicated, constant-area test section. Instead, a model is located at the end of the nozzle, which doubles as the test section.
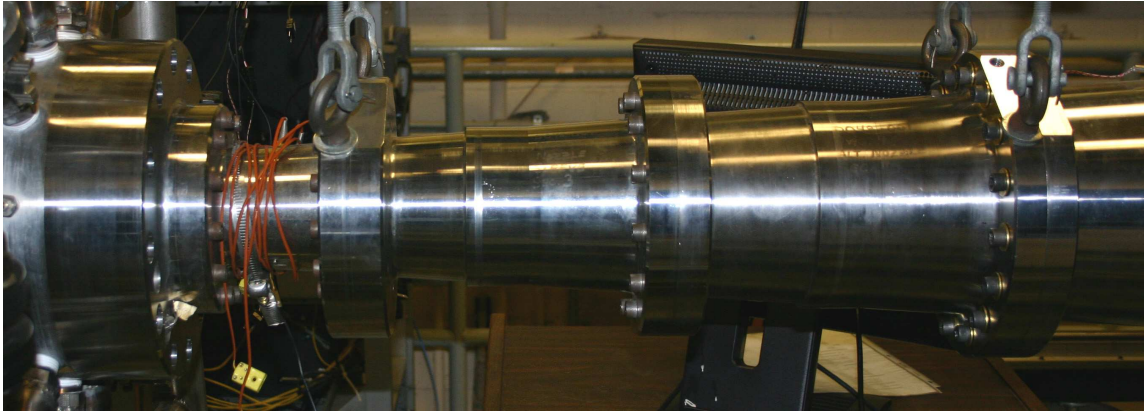
Figure 2.3: Electroform Sections 1 through 4 of the BAM6QT nozzle
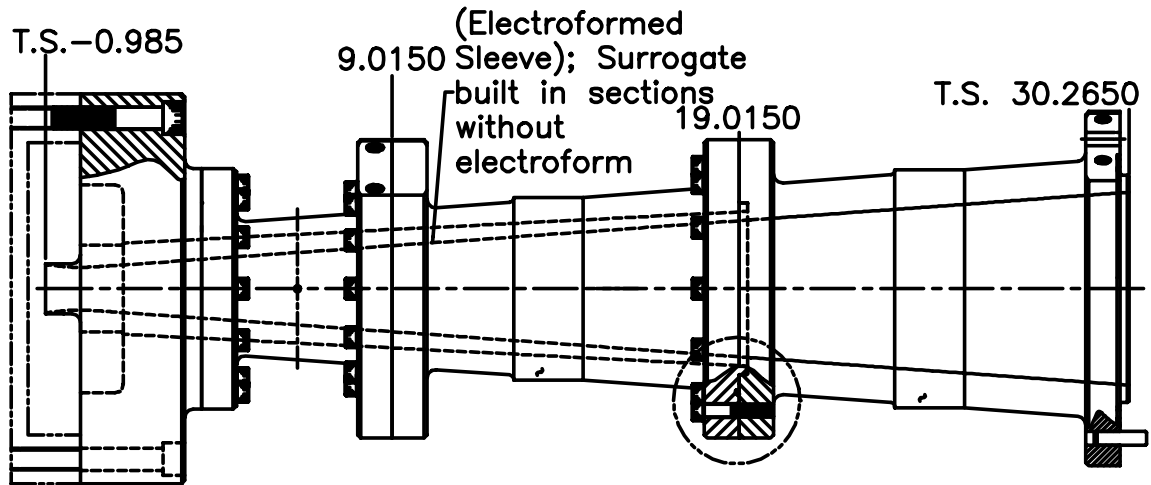
Figure 2.4: Schematic of Sections 1 through 4 of the BAM6QT nozzle

The last section of the nozzle, Section 8 (Figure 2.7), has several ports for various instruments and windows. A solid steel blank, a large acrylic window, and a smaller porthole window can be inserted in the large side port. No optical access was required
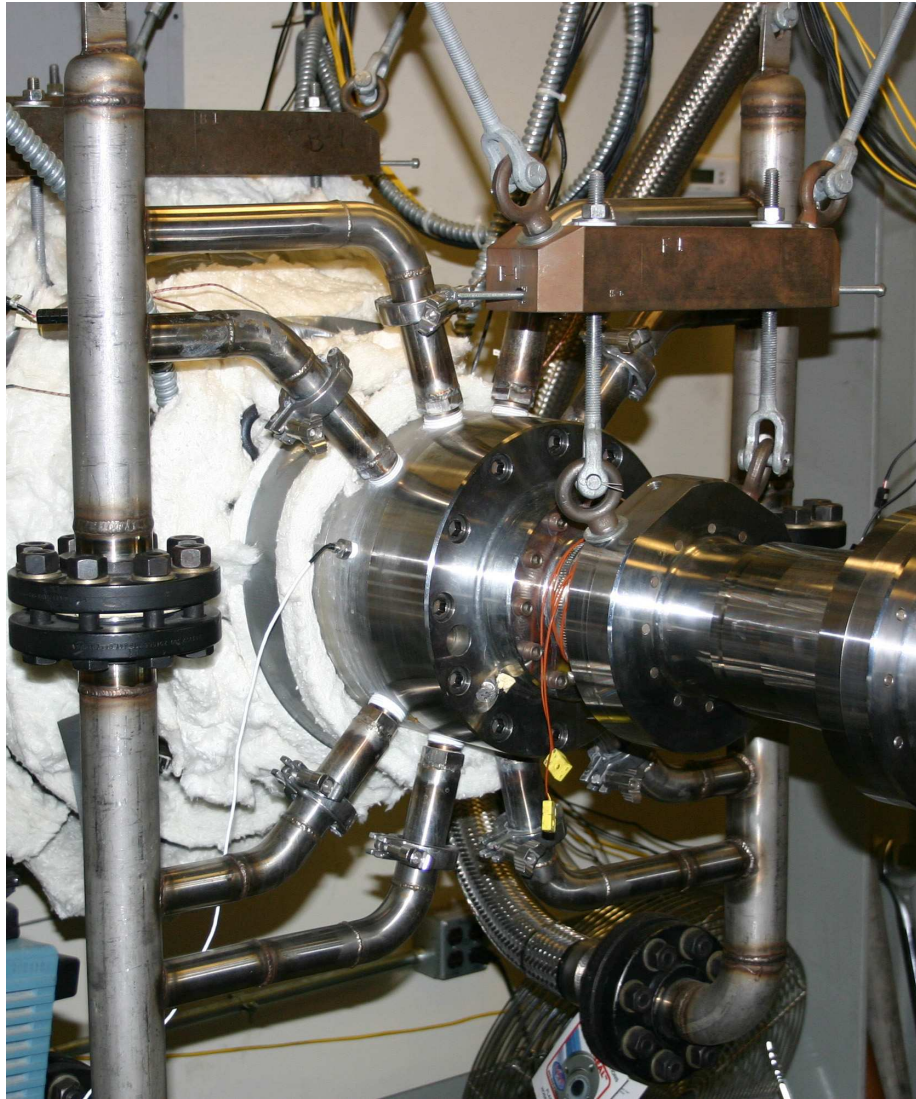
Figure 2.5: Contraction and bleed tubes
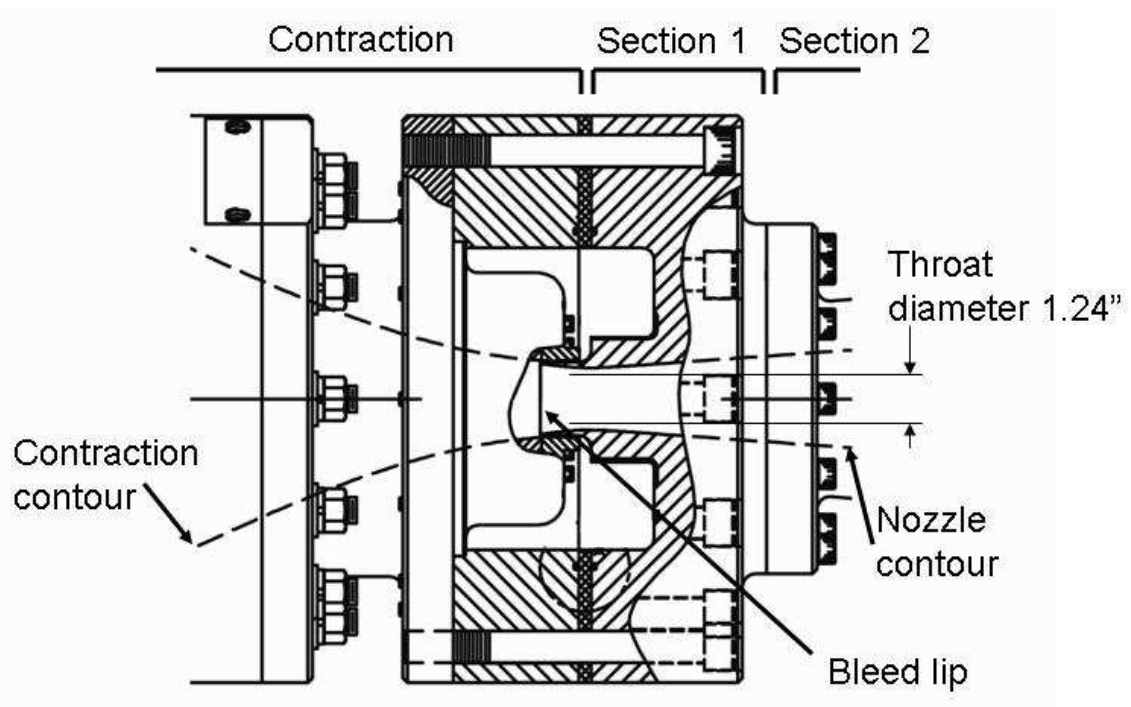
Figure 2.6: Cut-away drawing of contraction and nozzle

for this work, so these inserts were used interchangeably, with one exception. The large acrylic window is limited to a maximum of 138 psig and was therefore swapped out for one of the others during the pressure tests. The traverse system is installed in the aft-upper Section 8 port (see section 2.5). The far-forward pitot (section 2.2) and hot-film array (section 2.3) inserts are options for the forward-lower port.
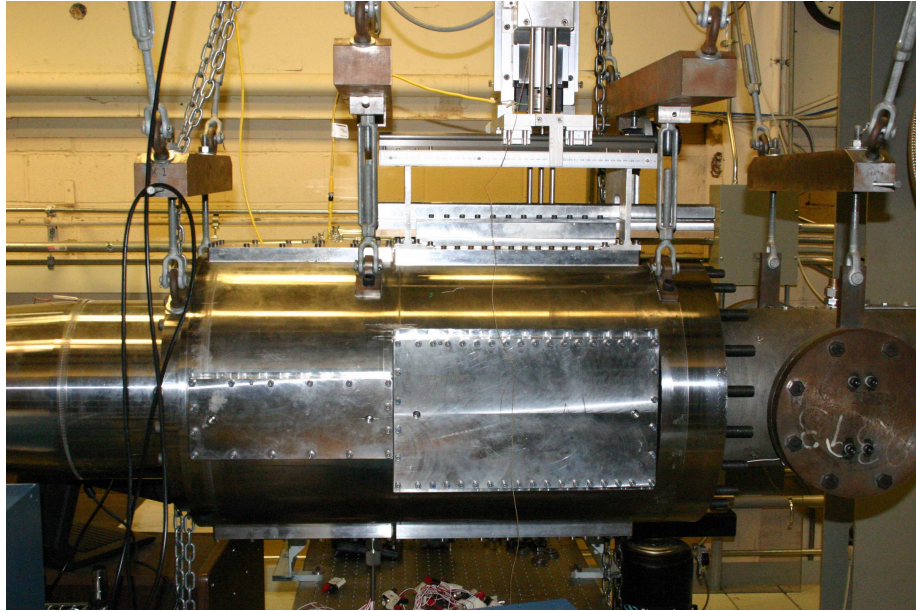
Figure 2.7: Section 8 with steel blank window inserts

Downstream of the test section is the 12-in.-diameter diffuser, where the bleed slot air can reenter the flow. The model sting mount is bolted into the first section of the diffuser. The model itself is attached to a sting that extends forward into the nozzle. Downstream of the diffuser is the diaphragm section. Finally, a large gate valve and more 12 in. piping (including the sliding sleeve) leads to the 4000-cubic-foot vacuum tank. The sliding sleeve (Figure 2.8) is a pair of 4-ft.-long pipes, one with an outer diameter 0.02 in. smaller than the inner diameter of the other. O-rings maintain a seal between the two pipes as they slide relative to one another. A pair of hydraulic rams with an associated pump provide the force to extend and retract the

sleeve. This setup allows the tunnel to be opened in order to change diaphragms, models, or larger hardware (such as the nozzle).
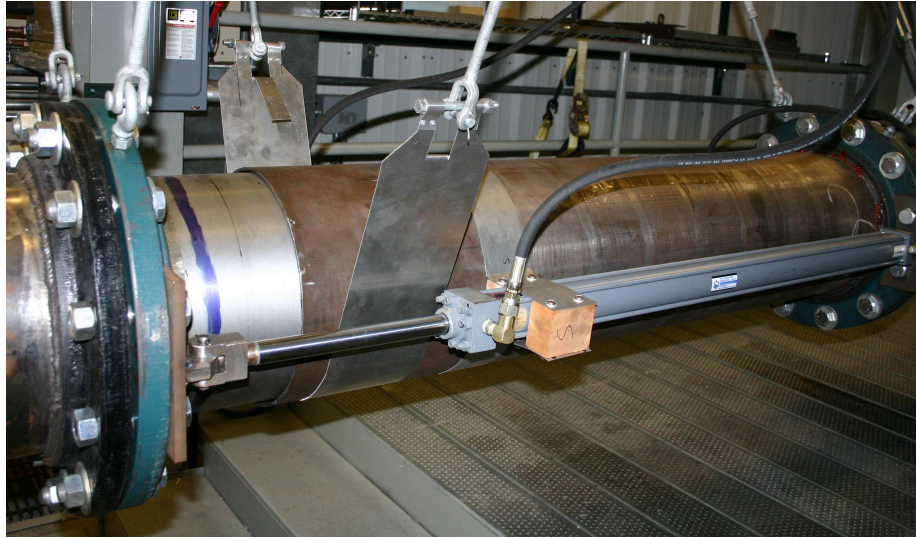
Figure 2.8: The sliding sleeve

Two diaphragms are used in every run. The diaphragms are discs of aluminum or acetate 13.6 in. in diameter and 0.008 in. to 0.040 in. thick. A set of diaphragm rings holds the diaphragms about 0.5 in. apart. The pressure in this gap is maintained at roughly half of the upstream pressure. Diaphragm material and thickness is chosen such that each can withstand a pressure difference greater than the gap pressure but less than the driver tube pressure. To initiate the run, the air in the gap is evacuated to the vacuum tank. The upstream and downstream diaphragms burst in rapid succession and the run begins. The remnants of the diaphragms blow into the vacuum tank, accumulate there, and are cleaned out annually.

2.2 Kulite Pressure Transducers

Kulite Semiconductor pressure transducers were employed in the contraction and in the test section. A flush-mounted model XTEL-190-200A transducer is located at the entrance to the contraction and, because the Mach number there is low, provides

the total pressure during the course of the run. This model transducer has a range from 0 to 200 psia. Model XCQ-062-15A transducers were mounted on pitot tubes in the test section and extend forward into the nozzle of the tunnel (Figure 2.9). The output from the pitot transducers was used to calculate the tunnel noise level. This transducer's range is 0 to 18 psia. A mechanical stop is placed behind the strain gauge so that it does not read higher pressures. This feature prevents damage that would otherwise be sustained at pre-run pressures greater than twice the operating pressure.
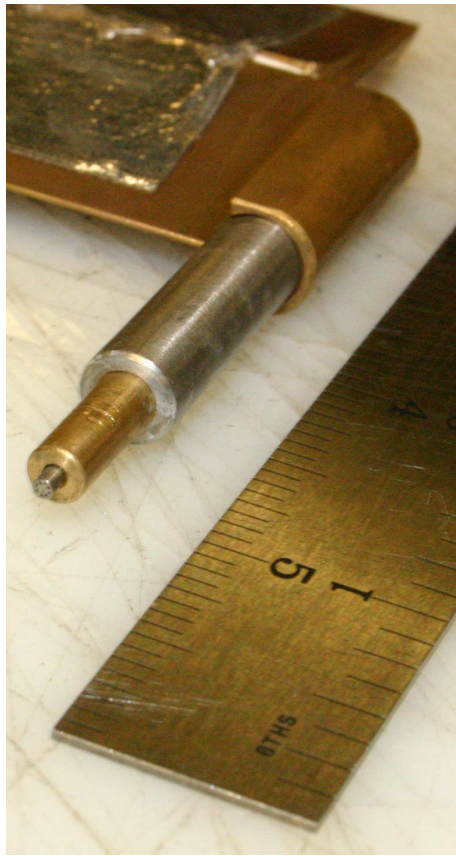
Figure 2.9: Pressure transducer in pitot mount

Custom-built electronics boxes condition the signals from the transducers. The transducer output is amplified by a gain of 100 using an INA103 instrumentation amplifier chip, and output as the DC signal. This amplified signal is then high-

pass filtered at 840 Hz and amplified again by 100 and output as the AC signal
(Figure 2.10). The DC signal is used to calculate the mean pressure for both the
contraction and nozzle. The pitot AC signal is needed to calculate the nozzle noise
levels, especially when the flow is quiet, due to the low signal-to-noise ratio.
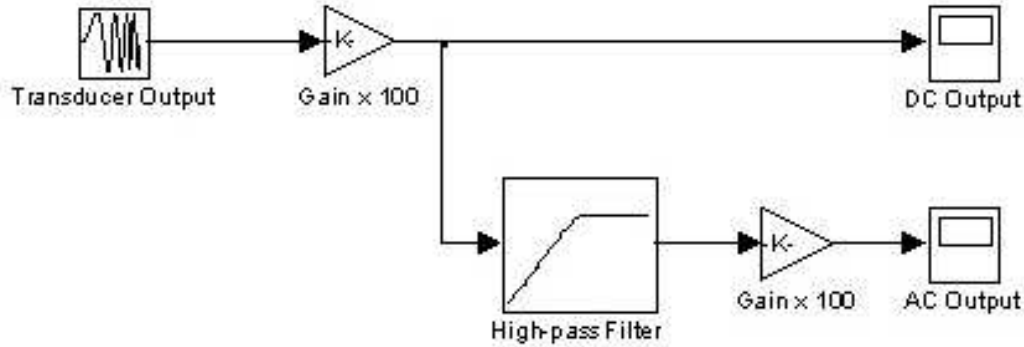
Figure 2.10: Kulite electronics diagram

Before each session in the tunnel, the transducers were calibrated with a Paro-
scientific, Inc. Model 740 Digiquartz Portable Standard over the range of pressures
to be tested. A linear regression fit gave squared correlation coefficients $R^2 > 0.999$
for both transducers. Variations in the slope from week to week were less than 1%.
Figure 2.11 contains typical transducer calibrations along with the linear regression.
Table 2.1 contains the equations of the best fit lines of the form $V = a * P + b$.

Table 2.1: Contraction & pitot pressure transducer calibration

Transducer	a (V/psia)	b (V)
Contraction	0.042316	−0.110111
Pitot	0.578806	0.207121

Four different pitot pressure transducer mounts were used. The far-forward pitot
extends forward into the nozzle from its mount, an insert for the lower-forward port
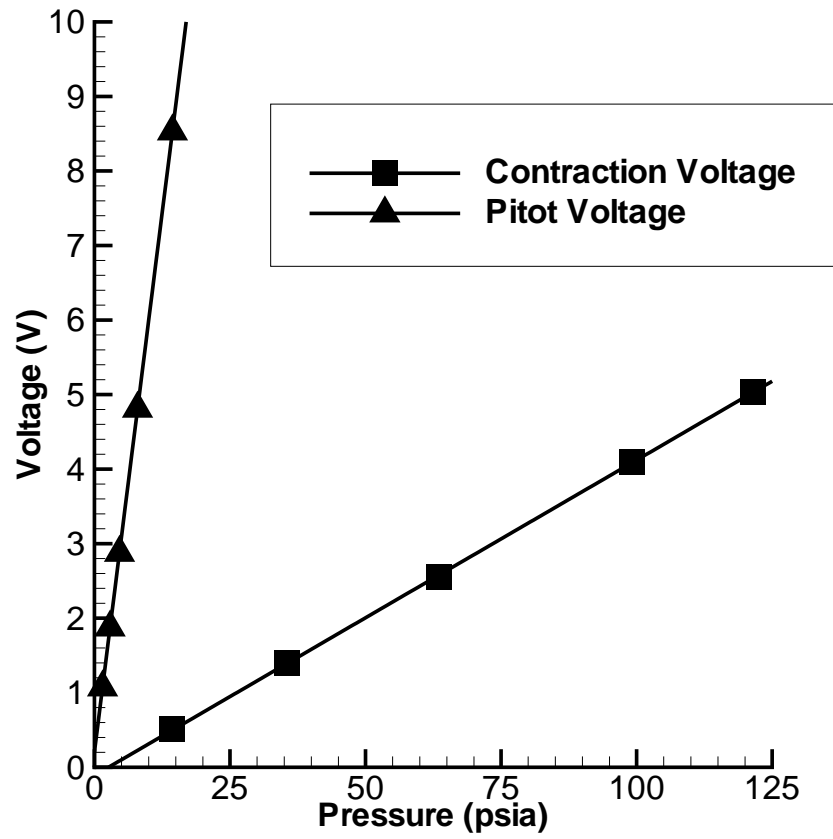
Figure 2.11: Contraction & pitot pressure transducer calibration

in Section 8. The far-forward pitot is located at $z = 1.15$ m downstream of the throat, along the centerline of the tunnel. The other three pitots are mounted in the traverse, which is installed in the upper-aft Section 8 opening (Figure 2.12). The short pitot is 6.6 cm long and can traverse vertically from 2.3 cm below to 10.2 cm above the centerline. The two long pitots are 30 cm long. One can cover the upper half of the test section, and the other the lower half.

Figure 2.12: Traverse pitots

2.3 Hot Films

In order to detect separation of the nozzle-wall boundary layer, Dr. Craig Skoch installed a Senflex hot-film array on an insert for the forward-lower port of Section 8, the last section of the nozzle (Figures 2.13 and 2.14) [29]. The hot films are controlled by Bruhn-6 Constant Temperature Anemometers built at Purdue. The system was employed in the same way as in Dr. Skoch's work, but at higher quiet

pressures than available at the time. The hot films were not calibrated. Laminar and turbulent boundary layers and separation were easily identifiable nonetheless (see section 6.3).
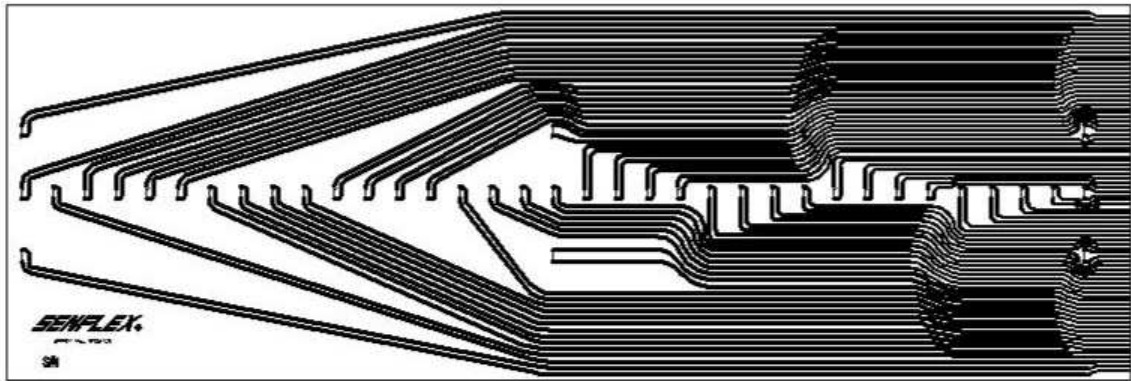
Figure 2.13: Diagram of hot-film array (9 in. by 3 in.)

Figure 2.14: Hot-film array installed in Section 8

2.4 Tektronix TDS 7104 & 5034 Oscilloscopes

All contraction and pitot pressure transducer readings were recorded on an 8-bit Tektronix TDS 7104 Digital Oscilloscope. The oscilloscope has enough memory to save 10 seconds of High-Res data at a 200 kHz sampling rate for each of four channels. The hot film data were recorded on a Tektronix TDS 5034 Digital Oscilloscope in Hi-Res mode at 100 kHz sampling. When the oscilloscope is set to Hi-Res mode, it samples at 1 GHz then averages the data on the fly and saves it at the set sampling frequency, supplying 11-12 bits of resolution and digital filtering.

The oscilloscope was set to record ten seconds of data. The drop in pressure detected by the pitot transducer was used as a trigger for the beginning of the run. Whenever a second oscilloscope was employed, it was triggered from the first. One second of pre-run data was saved as a reference for electronic noise.

In all cases, the vertical scale was set to optimize resolution for the relevant data. This choice has two noteworthy side effects. For the pitot DC pressure reading, the pre-run and trigger voltage levels were off-scale high. The oscilloscope is still able to recognize the voltage drop and triggers reliably. Also, in order to accurately measure quiet fluctuations, the pitot AC pressure level is off-scale both high and low when the flow is noisy or a turbulent spike occurs. The DC pressure has enough resolution to calculate the noise level for noisy flow. The Matlab code written to calculate the noise level uses the appropriate data in its calculations by first using the pitot AC pressure and then, if the noise level is high, switching to the DC pressure data (Appendix A.1).

2.5 Probe Traverse

The pitot-mounted pressure transducer is attached to a Parker Square Rail Positioner that is driven by a Parker stepper motor (Figure 2.15) [30]. The hardware is controlled by Parker Compumotor Motion Planner software running on an attached PC. For most tunnel runs, the pitot was located within 2 mm of the tunnel center-

line. Careful use of a simple six-inch ruler and increasingly-fine adjustments in the location permitted centering the probe in about two minutes. For tests of the flow symmetry, the probe was first centered and then the proper radial offset was entered into Motion Planner. For both of these cases, the probe was stationary during the run. During the tests with a cone model, the probe was traversed through the shock during the course of the run. A Fortran script was obtained from Erick Swanson to create the series of instructions for Motion Planner to move the probe. When the oscilloscope triggers from the drop in pitot pressure, it sends a signal to the Motion Planner software to execute the program.
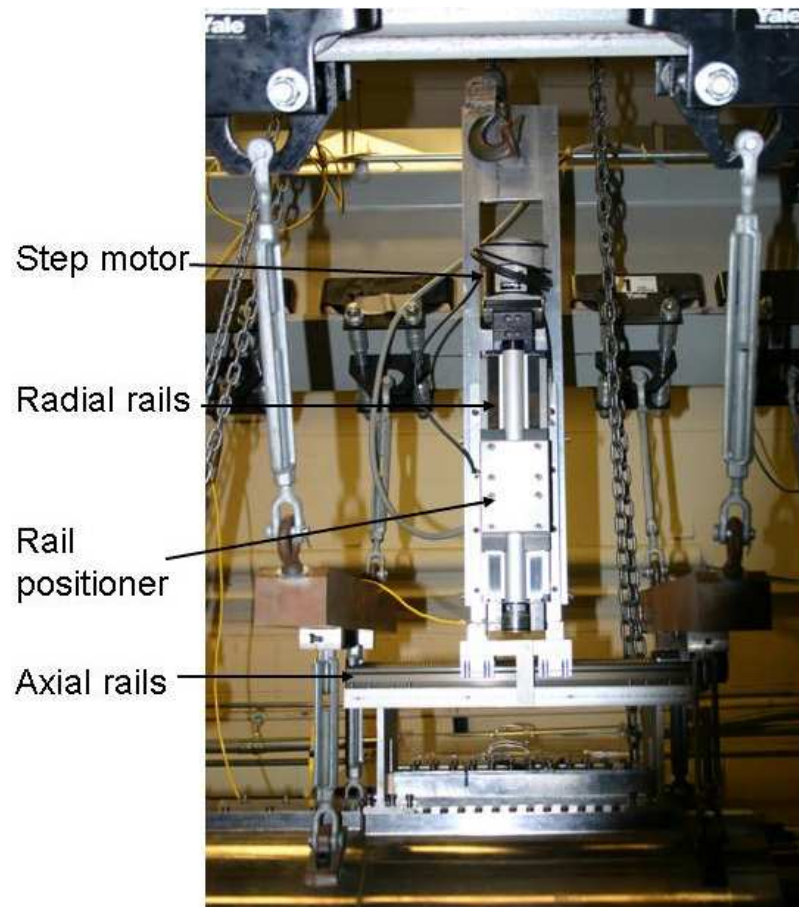
Figure 2.15: Probe traverse

3. Preliminary Results

3.1   Pressure Tests

Pressure tests of the surrogate nozzle were conducted on three occasions to set and then increase its maximum allowable working pressure (MAWP). The original MAWP for the surrogate, 88 psig, was calculated with the same (very conservative) temperature assumptions ($T < 300$ °F) as used for the steel, but with the material properties of aluminum (29% the strength of steel at that temperature). The tunnel pressure was increased to 150% of the MAWP, 132 psig, and held there for 40 minutes. Leak tests were made with diluted liquid soap that would bubble at the location of a leak. No leaks were detected.

Thermocouples were attached to the outer surface of the surrogate nozzle at several locations near the upstream end. The highest temperature any one detected was 63 °C (153 °F). For an operating temperature of 200 °F, the MAWP is 107 psig (121.5 psia). Once again, the nozzle was pressurized to 150% of the MAWP (161 psig or 175 psia). The boost pump was employed to reach pressures above 145 psia. No leaks were detected after one hour at 161 psig.

In February 2006, the tunnel ran quietly above the then-current MAWP. The limiting component was the strength of the bolts between Sections 3 and 4, which have a safety factor of 11.4 at 200 °F. Increasing the MAWP from 107 psig to 180 psig reduces the safety factor to 6.8, which is still above the minimum safety factor of 5. The nozzle's maximum temperature of less than 200 °F occurs near the throat, but the temperature is less by Section 4, so the safety factor is actually greater than 6.8. Thus, runs up to 195 psia and a pressure test to 270 psig were approved. The pressure regulator that allows air into the driver tube would not fill above 276 psia.

The test was completed and no leaks were detected for $p > 270$ psia, increasing the MAWP to 185 psia.

3.2   CFD Analysis

CFD analysis by Doyle Knight et al. at Rutgers University indicates the presence of a separation bubble on the original, hemispherical bleed lip (Figure 3.1) [31] – [32]. This separation bubble could act as roughness that might trip the boundary layer to turbulent. The bubble is present very near the tip of the bleed lip, where the boundary layer is at its thinnest. There are separation bubbles predicted on both the main-flow and bleed-flow sides of the lip. The bleed-side bubble is not a concern because the flow in the bleed plenum was designed to be supersonic, so disturbances do not travel upstream.

A trade study on the bleed lip contour was performed by Selin Aradag and a new, elliptical bleed-lip profile was suggested to minimize the separation bubble [33]. The electroformed nickel nozzle was modified to the new profile in May 2006.

3.3   High-Precision Bleed Lip Geometry Measurement

In June and July 2005, Anderson Tool & Engineering Co. of Anderson, IN measured the bleed lip geometries of the surrogate aluminum and electroformed nickel nozzles. The radial coordinate was measured at 0.002 in. spacing around the bleed lip at four azimuthal locations (Figures 3.2 and 3.3).

Whereas the surrogate nozzle profiles at all azimuths are within 0.001 in. of one another, the 90° electroform profile deviates from the 0° and 180° profiles by more than 0.002 in. (Figure 3.4). In particular, at $z = 0.973$ in., where the radius should be 0.694 in., there is a definite 'kink' in the inner contour where the radius increases rather than smoothly decreases.

It has been suggested that the defect is a result of an error during the fabrication process. The nickel was deposited onto a mandrel; when the mandrel was removed
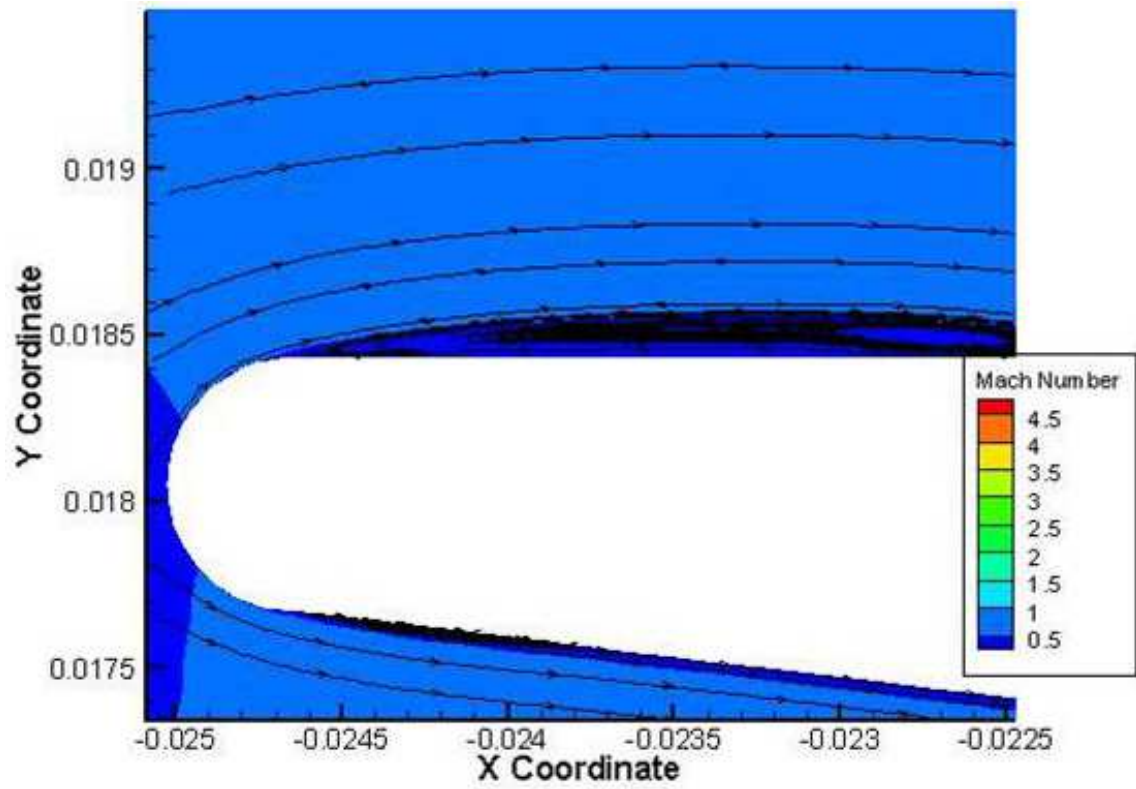
Figure 3.1: CFD results showing separation bubbles (Ref. [33])
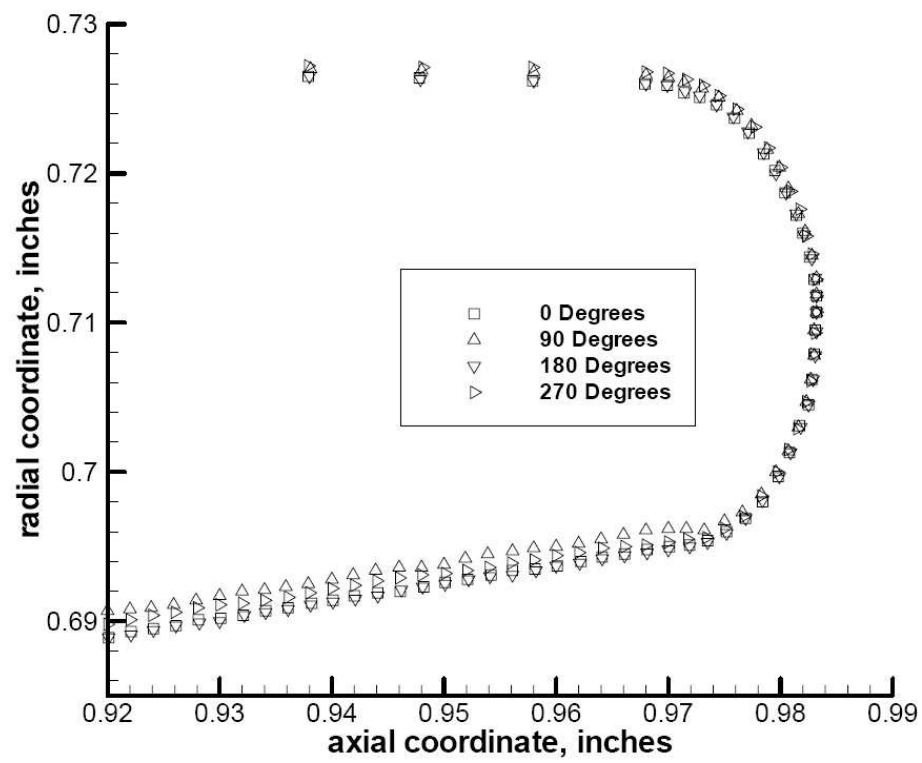
Figure 3.2: Electroform bleed lip geometry measurement (Ref. [34])
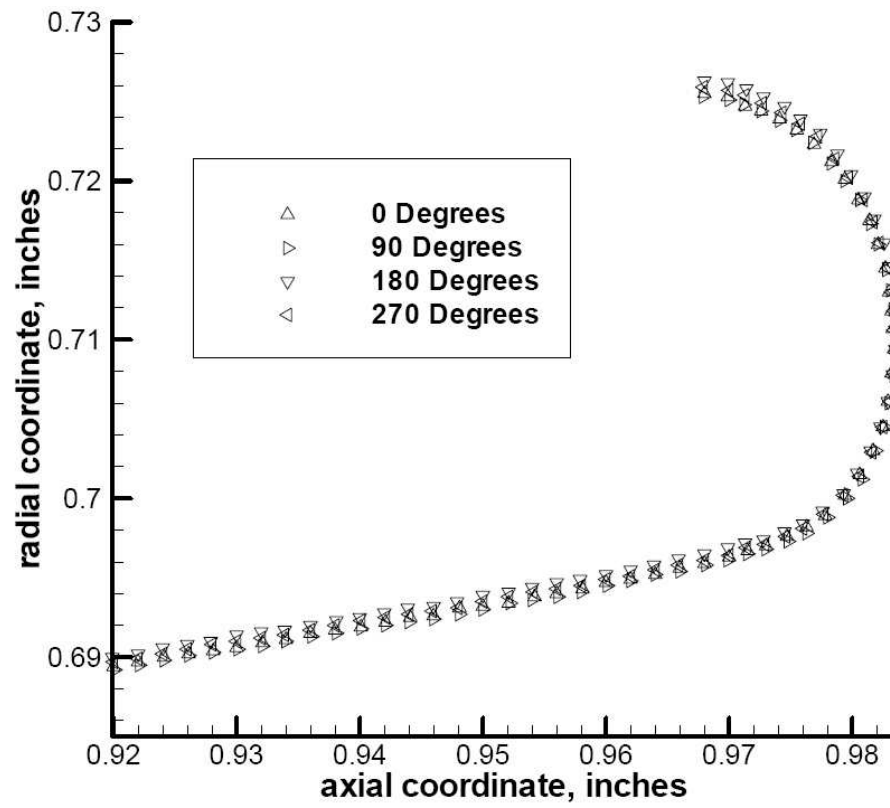
Figure 3.3: Surrogate bleed lip geometry measurement (Ref. [34])
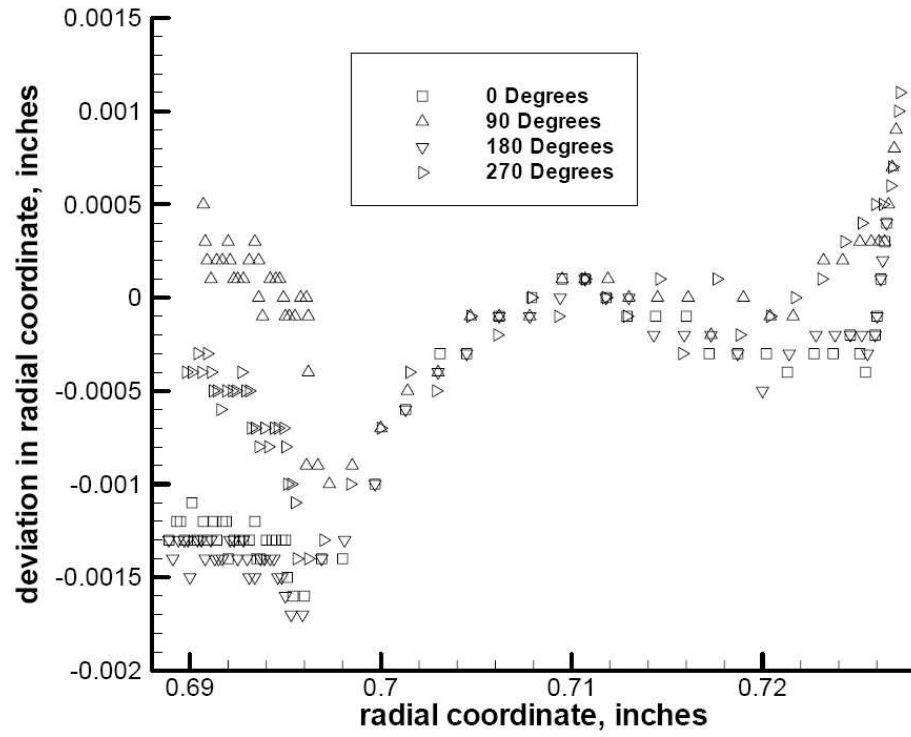
Figure 3.4: Deviation in nozzle radius; large deviation for $r < 0.696$ in. corresponds to kink location

from the nozzle, it distorted due to residual stresses. However, the lip was machined on a lathe as if it was axisymmetric, creating the flaw. This kink may be the bump noticed in 2002 [26]. Because it is so far upstream in the nozzle, where the boundary layer is at its thinnest, it is possible that this defect could be causing early transition in the nozzle wall boundary layer, due to the separation bubble shown in Rutgers computations [33]. The lack of a kink is the only known way in which the surrogate is superior to the electroform, which has a much better surface finish and no internal seams at the first three joints. Thus, it is likely that it accounts for the very low maximum quiet pressure of the electroformed nozzle.

In May 2006, the bleed lip of the electroformed nozzle was remachined by ATK/GASL into an elliptical profile calculated to minimize separation. Measurements made by ATK before and after the modification confirm the kink and show how it is eliminated (Figure 3.5).
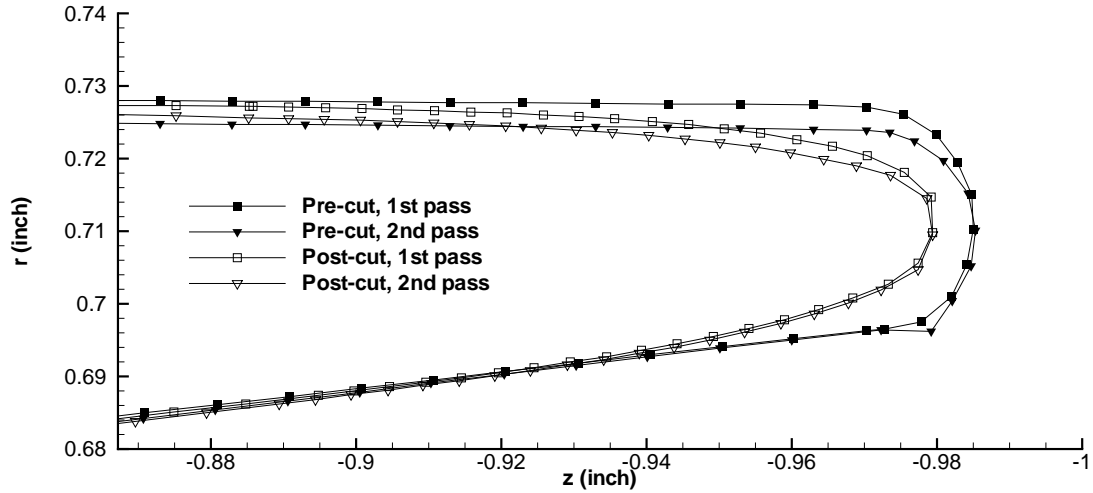
Figure 3.5: Pre-cut and post-cut measurements of bleed lip profile by ATK at two different azimuthal locations (Ref. [35])

4. Representative Data Analysis

4.1 Typical Oscilloscope Trace

Four pieces of data were collected from each tunnel run on the oscilloscope at a rate of $2 \cdot 10^5$ samples per second: the pressure in the contraction, the pressure in the bleed-suction plenum, the pitot pressure in the nozzle, and the high-frequency (AC) component of the pitot pressure. With this information, the maximum quiet-flow pressure for the particular run can be calculated. Figure 4.1 shows calibrated data from a typical run.
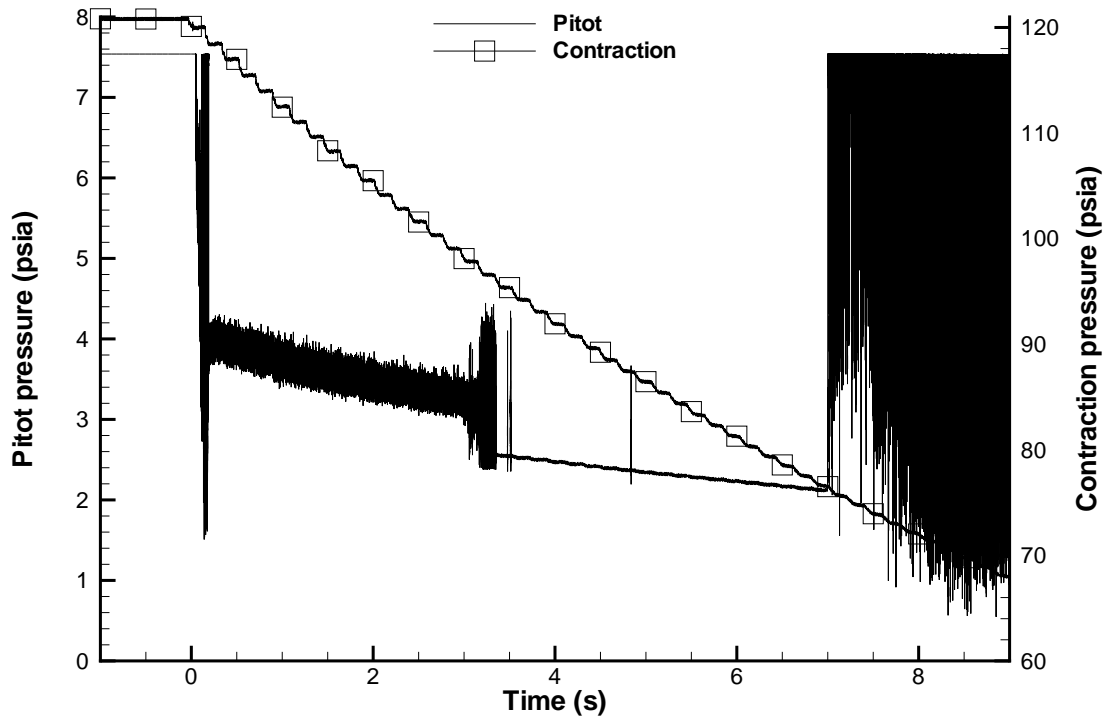
Figure 4.1: Typical pitot & contraction pressures

The oscilloscope records data for ten seconds and is triggered by the sudden drop in pitot pressure when the diaphragms burst. The first second of data is pre-run; time $t = 0$ s corresponds to the diaphragm burst and run start. During this run, the tunnel runs at high noise level until $t = 3.4$ s. The contraction pressure at which the noise level drops significantly (the quiet pressure) is 95.5 psia. With the exception of turbulent bursts at $t = 3.5$ and 4.8 s (see section 4.3), the tunnel is quiet until the run ends at $t = 7$ s. The transducer output is off the oscilloscope scale for $t < 0$ and $t > 7$ s, resulting in the misleadingly flat pressure maximum.

4.2   Noise Levels

The pressure data are also used to calculate the tunnel noise level $(\tilde{p}/\bar{p})$. See Appendix A.1 for the Matlab code written for this purpose. The noise level for the above run as a function of contraction pressure is shown in Figure 4.2. The data was divided into 0.1 s intervals for the calculation of $\tilde{p}$ and $\bar{p}$. Thus, $2 \cdot 10^4$ pressure values are used to evaluate each data point.

The pre-run ($p_t > 120$ psia) DC noise level is zero because the pitot pressure transducer is at its maximum reading. The root-mean-square AC voltage is typically 1.3 ± 0.3 mV and the pre-run noise level is less than 0.00035%. No attempt was made to subtract the background electronic noise. The noise increases to 2.5–2.8% until $p_t = 98$ psia, at which point the noise increases to above 12% during the series of turbulent bursts. When $p_t < 96$ psia the noise level decreases below 0.05%, except for occasional turbulent bursts (Figure 4.3). The noise level during the quiet portion of the run is a factor of fifty times less than the noisy portion. During the quiet portion of the run, the rms AC voltage is 30 to 50 mV, for a signal-to-noise ratio from 20 to 50. The noise level increases dramatically when the run ends ($p_t < 77$ psia).

The modifications made to the tunnel did not change the basic pattern of pitot pressure vs. time or the noise level vs. contraction pressure. Thus, after most runs data analysis consisted simply of applying the transducer calibrations to the oscillo-
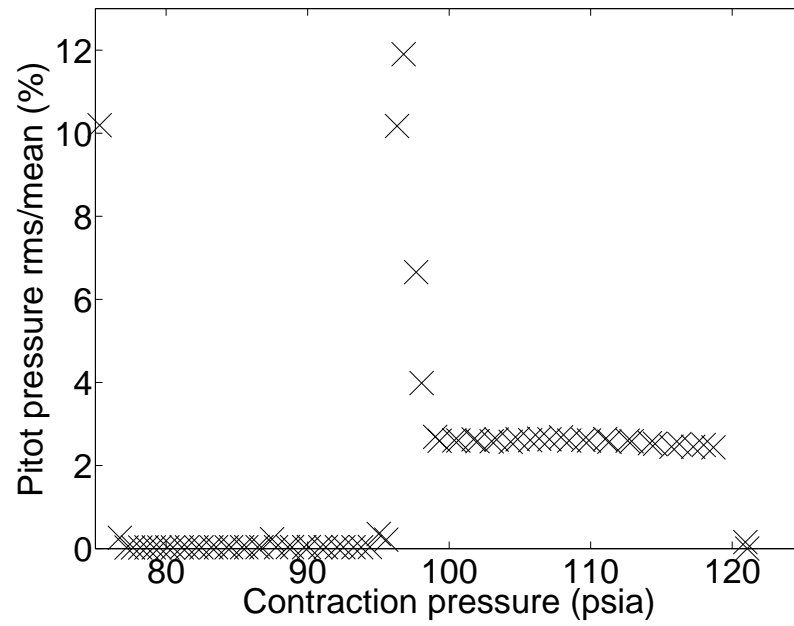
Figure 4.2: Typical noise level during a run
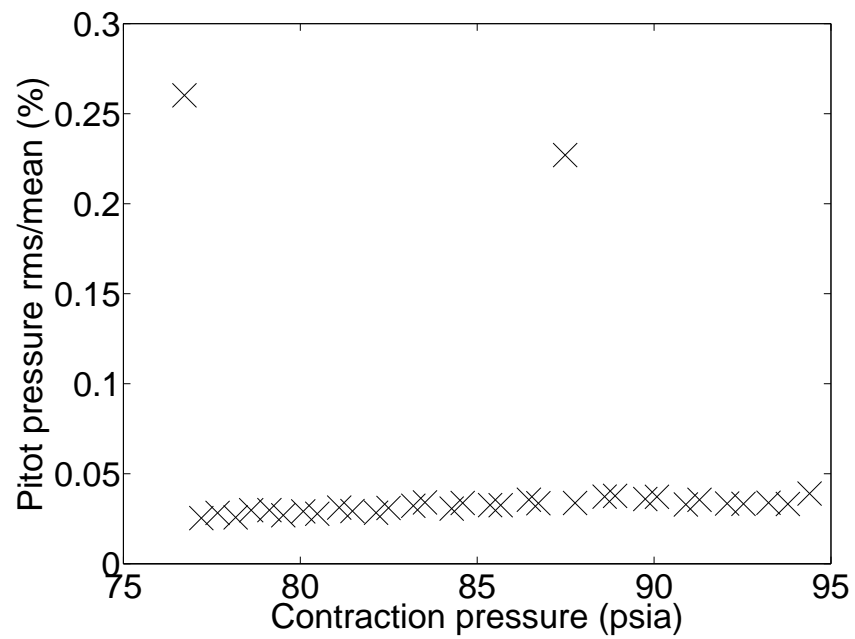
Figure 4.3: Typical noise level during quiet portion of a run

scope data and identifying the maximum quiet pressure for that run. The reduction in noise level at the onset of quiet flow is quite pronounced and easily ascertained.

4.3 Turbulent Bursts

During the quiet portion of most runs that had one, one or more short-duration pressure spikes would occur. These bursts all had a similar structure, such as the one in Figure 4.4. Less than 0.0015 s elapses between the onset of the spike and the pressure minimum, then the pressure increases back to the pre-spike level over the next 0.0035 s. The magnitude of the pressure spike is proportional to the stagnation pressure for the run and is greater than the pressure variation during noisy flow.
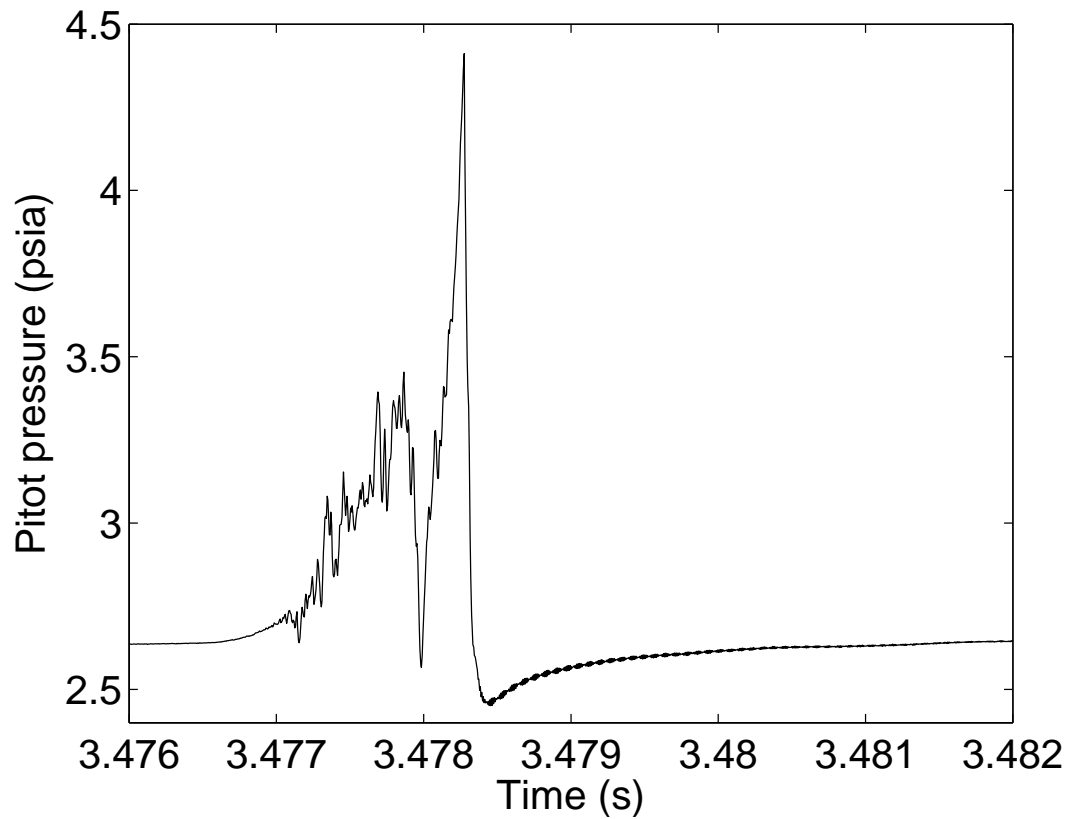
Figure 4.4: Turbulent burst

The burst is probably due to a disturbance from a small spot of turbulence on the nozzle wall. The pitot pressure trace at the time of the change from noisy to quiet flow shows that a series of bursts is just before the flow becomes quiet (Figure 4.5). Regular noisy flow, on the other hand, is a normally distributed band (Figure 4.6). It is reasonable to assume that these bursts are the result of a turbulent nozzle-wall boundary layer becoming intermittently turbulent before laminar.
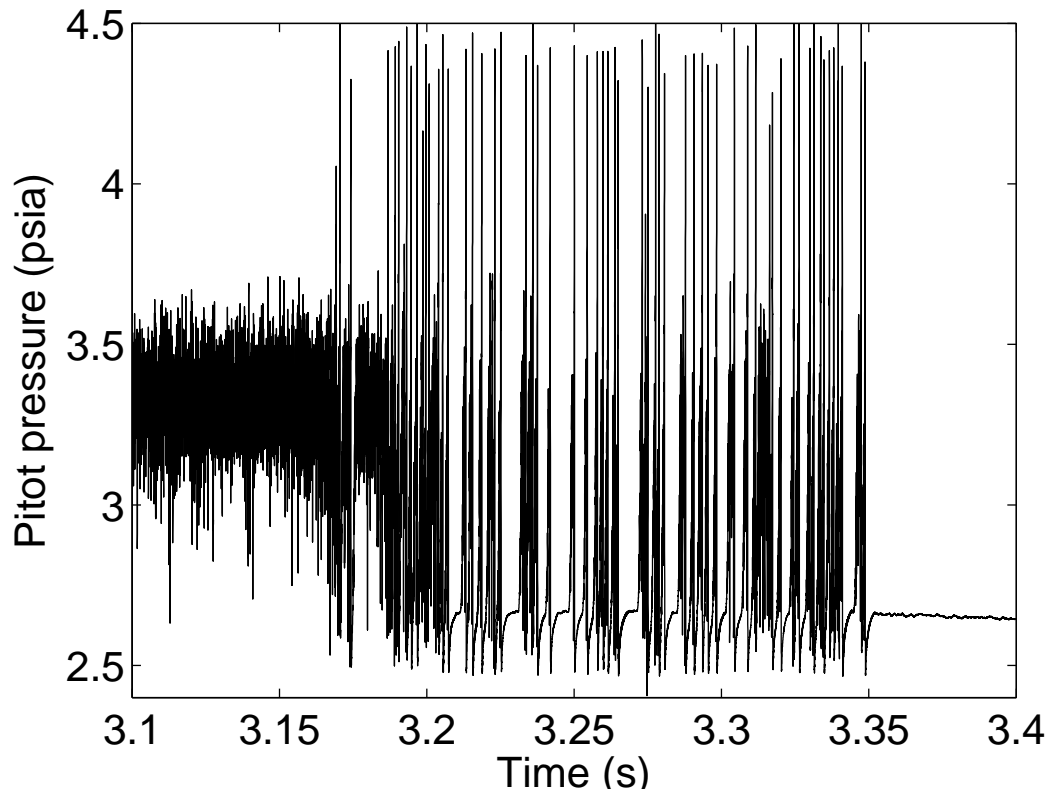
Figure 4.5: Turbulent bursts at onset of quiet flow

With the surrogate nozzle, there will occasionally be a run with a large number of bursts during the otherwise quiet period (more than two per second on average). This problem could not be predicted before a run or replicated during subsequent runs. The electroformed nozzle has fewer bursts during the quiet period than the
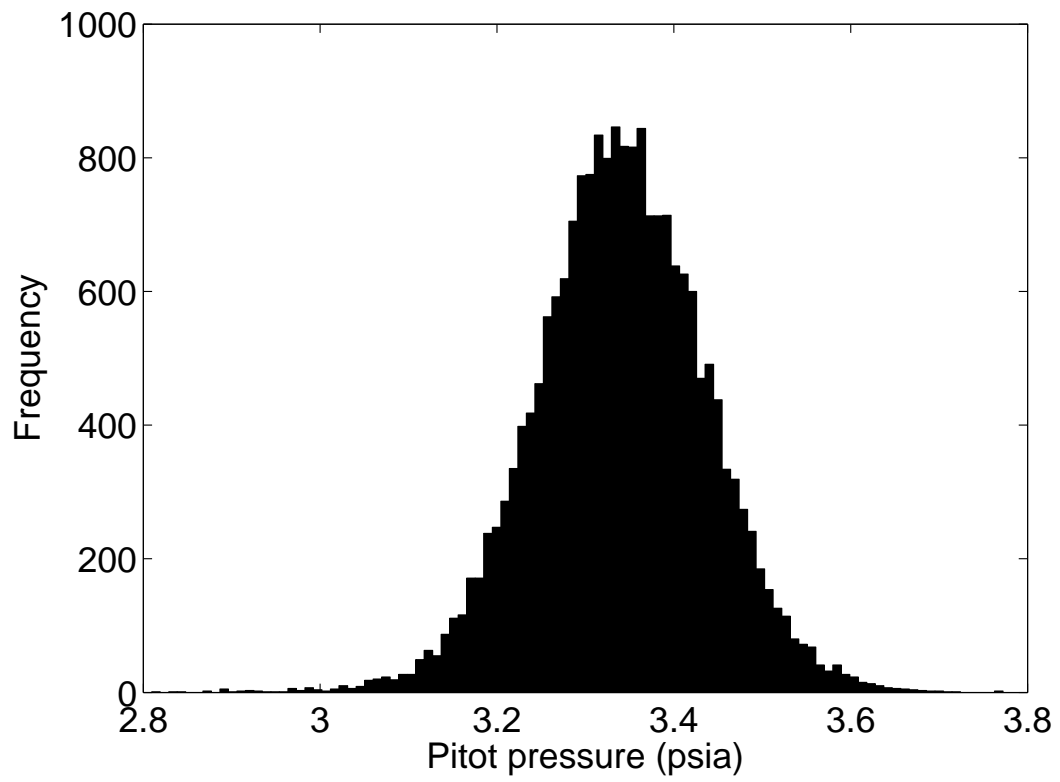
Figure 4.6: Pressure distribution for 0.1 s of noisy flow

surrogate. This improvement could be due to its better polish or lack of seams between the first four sections.

4.4   Mach Number

The Mach number at a particular pitot location and time during the run is calculated with the Rayleigh Pitot formula, which calculates the ratio of stagnation pressures across a shock as a function of upstream Mach number.

$$\frac{p_{01}}{p_{02}} = \left(\frac{(\gamma+1)^2 M^2}{4\gamma M^2 - 2(\gamma-1)}\right)^{\frac{\gamma}{(\gamma-1)}} \cdot \left(\frac{1-\gamma+2\gamma M^2}{\gamma+1}\right) \tag{4.1}$$

This formula is not explicit for M, so a bisector method is used to solve for it from the contraction and pitot pressures (Appendix A.2). Laminar boundary layers are thinner than turbulent ones [36], so the effective area ratio between that location in the nozzle and the throat (A/A^*) is larger. If the assumption of quasi-one-dimensional flow is made, the Mach number at a location is a function solely of this area ratio and the ratio of specific heats:

$$\frac{A}{A^*} = \frac{1}{M}\left(1+\frac{\gamma-1}{2}M^2\right)^{\frac{\gamma+1}{2(\gamma-1)}} \cdot \left(\frac{2}{\gamma+1}\right)^{\frac{\gamma+1}{2(\gamma-1)}} \tag{4.2}$$

Therefore noisy flow in the test section is at a lower Mach number than quiet flow. Separated flow (section 6.3) has an even bigger influence on the effective A/A^*, and will cause a larger decrease of the Mach number. The plot of Mach number versus contraction pressure or time provides another means for determining if the flow is noisy or quiet (Figure 4.7). This run is noisy for the first 2.2 s, during which the Mach number is about 5.6. The flow is quiet briefly and the Mach number increases above 5.9. The flow separates during $2.5 < t < 4.0$ s and the Mach number drops accordingly to about 5.0. The flow reattaches and remains quiet for the remainder of the run, while the Mach number is between 5.9 and 6.0.
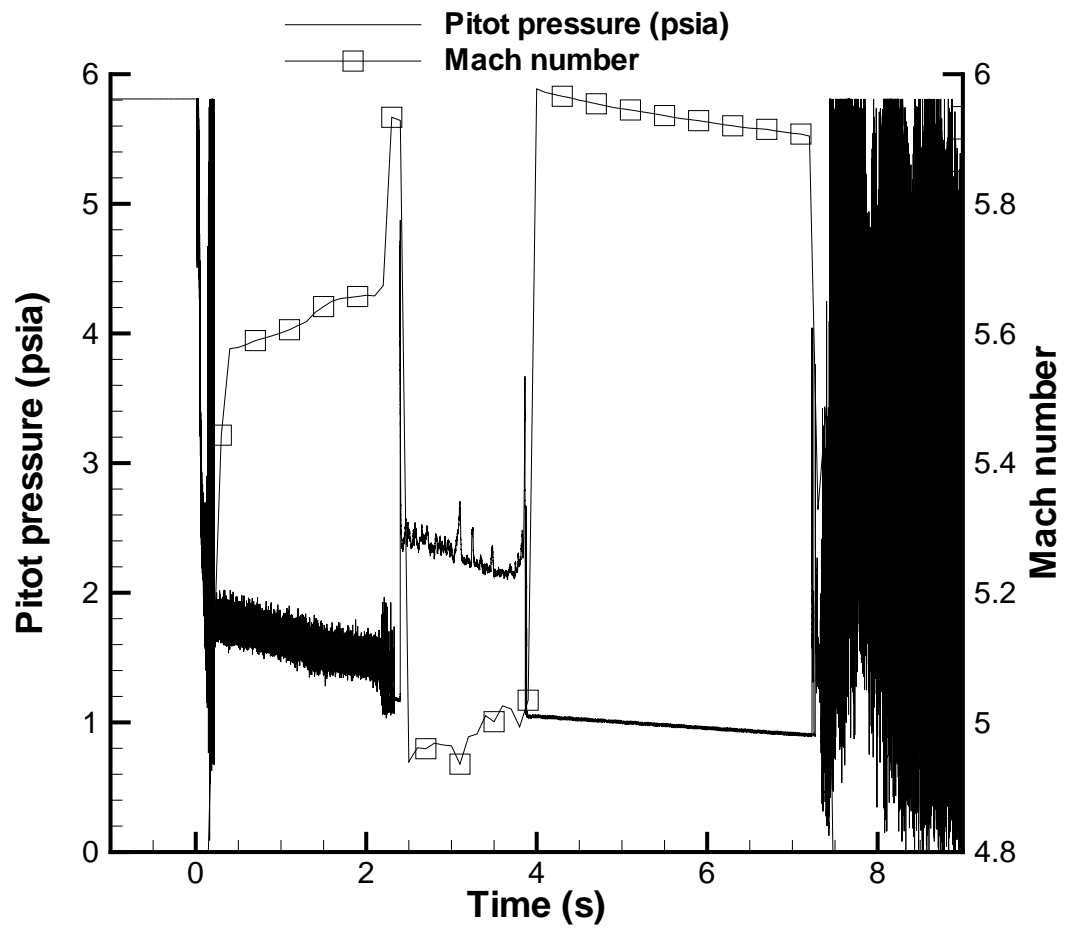
Figure 4.7: Typical Mach number for run starting at $p_t = 45$ psia

5. Nozzle Modifications and Their Effect on Performance

5.1   Chronological Account

The original, electroformed throat never ran quietly for $p_t > 8$ psia. At the suggestion of Professor Garry Brown of Princeton University, a surrogate throat made of aluminum was made to the same nominal design but with the intention of modifying it with additional sensor access and a redesigned bleed lip. The surrogate nozzle was completed in January 2005 and first tested in February by Matt Borg. Initial runs indicated that flow through the surrogate nozzle throat was quiet for $p_t < 20$ psia. This improvement came as a surprise because the aluminum was much less highly polished than the electroformed nickel [34].

At this time, an aft-facing step was noticed between Sections 4 and 5 (at the interface between the surrogate and the original nozzle). Jerry Hahn of the ASL shop increased the inner diameter at the end of Section 4 by 0.0044 inches and faired it smoothly to the rest of the section. This modification was tested in late June 2005 and yielded a quiet pressure of 37 psia.

The next change made to the surrogate was to have it polished by Optek, Inc. of Batavia, IL. The polish gave a dramatic improvement to the inside finish. Unfortunately, during the installation of the surrogate, the bleed lip was nicked (Figure 5.1). The next set of tests, during late August 2005, assessed the effect of the nicks. The first tests after the damage gave quiet flow only below 12 psia. Mr. Hahn hand-polished the nozzle, improving its quiet limit to 34 psia, which was still lower than before the polish.

The surrogate nozzle was taken back to Optek for repair. They concentrated near the throat and extended the polished region around the bleed lip. The nozzle was returned and installed for tests in late September 2005. These tests yielded quiet

Figure 5.1: Polished surrogate throat with nicks on bleed lip at 7 o'clock

flow for $p_t < 94$ psia. The surrogate nozzle was swapped out for the electroform and reinstalled in early November, 2005. Initially, the quiet pressure was the same as before. However, during the fourth run of the week, the maximum quiet pressure dropped to 73 psia. There is no obvious explanation for this change.

Once again, the surrogate nozzle was removed and stored in its crate while the electroform was in use. In January 2006 the surrogate was reinstalled and at first ran quietly for $p_t < 73$ psia. However, starting with the week's fifth run, the quiet pressure was back up to 92 psia. It has been suggested that there was dust in the nozzle that finally blew out. Oily streaks were observed on the nozzle walls and a bit of a glint was present at the seam between Sections 1 and 2 (Figure 5.2). The streaks did not change much between the installation of the nozzle and its removal two weeks later. Acetone was used to wipe away the streaks that could be reached.

(a) Glint   (b) Streaks
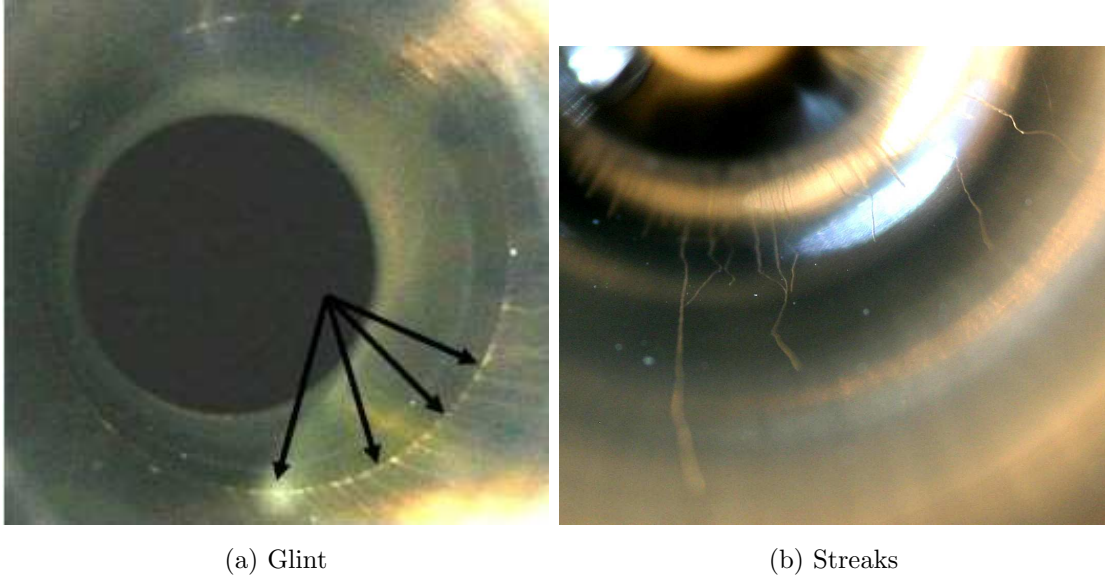
Figure 5.2: Observed imperfections on polished nozzle

The tunnel was twice cooled and reheated to see if there was any effect upon the maximum quiet pressure. The temperature cycles had the unintended effect of distorting the o-ring between two contraction sections at $z = -23.73$ in., causing a leak. The temperature cycles, the leaky contraction, or some other cause reduced the quiet pressure to 70 and then 54 psia.

The contraction o-ring and the bleed tube gaskets were replaced and the nozzles were swapped again before resuming testing on the surrogate in late January 2006. Surprisingly, the maximum quiet pressure had jumped to above 122 psia, the maximum allowable working pressure for the aluminum nozzle at the time. Several leaks were made in the contraction by loosening the upper and lower access ports. Even with 0.183-inch-diameter holes in the upper and lower ports, the tunnel was still quiet for the entire run beginning at $p_t = 122$ psia. Loosening one of the bleed suction tube connections also had no effect. These changes might have lowered the quiet pressure — just not below 122 psia. This robustness indicates that neither the leaky contraction o-ring nor old gaskets were the likely cause of the lower quiet pressures observed earlier.

The tunnel continued to run quietly below 122 psia for two weeks while Shann Rufer performed low-noise boundary-layer-instability tests on cones. A pressure test was done in February 2005 in order to approve the aluminum nozzle for higher allowable working pressures. After the test, the tunnel was quiet only for $p_t <$ 69 psia. The pressure test was repeated with no further change to the maximum quiet pressure. The tunnel was not opened at the throat before or after the pressure test, making dust contamination or misalignment unlikely.

The nozzle was detached before Section 1 (at the throat) and after Section 4 (at the end of the surrogate portion). Streaks of oily residue were again present, emanating from the seam between Sections 2 and 3. Wiping with acetone removed them easily. The uneven glint between Sections 1 and 2 first noted in early January was visible from both upstream and downstream ends. To reach the joint, several Kimwipes were rubber banded to the end of a two-foot-long balsa stick. The step was merely accumulated gunk and it came off onto the acetone-wetted Kimwipes. The face of the upstream flange of Section 1 was fairly grimy; acetone was again used to wipe clean the surface. The nozzle was realigned, reattached, reheated, and retested. The maximum quiet pressure decreased again, to 53 psia. The nozzle was detached and cleaned a second time. It was still very clean. After reattaching the nozzle and heating for about 24 hours it ran quietly below 58 psia.

Matt Borg was using the surrogate nozzle during the last week of February 2006. Starting with his very first run, the quiet pressure increased to 130 psia, the highest quiet pressure to date (August 2006) for the surrogate nozzle. The nozzle was not detached in the interim. One possibility is that extra time was needed for the nozzle to heat up. After several equally-quiet runs, he opened and closed the top and bottom contraction access ports in order to change hot wire location. The quiet pressure became just 31 psia. The nozzle was detached and cleaned as before. It was not particularly dirty and there were no readily visible scratches. Tests after reattachment (and heating for > 60 hours) showed quiet flow for $p_t < 50$ psia.

The electroformed nozzle was reinstalled for two weeks in the middle of March 2006, then replaced again by the surrogate. The surrogate appeared scratch-free and mostly clean but was wiped with acetone nonetheless. From the first run, the tunnel exhibited a maximum quiet pressure of 108 psia.

In April 2006, the surrogate was taken to Optek for more polishing. After several months of running, the aluminum polish had worn away slightly. It simply was not as shiny as it was after the previous polish, though it was still far better than before the original polish. Also, the seam at the joint between Sections 1 and 2 was visible. The nozzle was polished throughout with special attention at that joint. Also, a ding at the end of Section 4, probably the result of a tool bump during installation or removal, was repaired.

The surrogate nozzle was reinstalled and tested in late May. Initially, the flow was quiet for $p_t < 62$ psia. The nozzle was detached and cleaned. There was no grease to clean and the polish had not degraded. There was some dust in the nozzle that was probably from the tissue paper used to clean it. The nozzle was reattached and ran quietly only below 44 psia. This detach/clean/reattach process was repeated and the tunnel quiet pressure improved to 73 psia. This variability is similar to that experienced in February 2006, when simply opening and reclosing the nozzle achieved moderate fluctuations in performance.

ATK/GASL remachined the bleed lip of the electroformed nozzle into the elliptical profile provided by Professor Doyle Knight and Selin Aradag (Figure 3.5). The modified electroform was installed and tested in June 2006. The flow became quiet at $p_t < 39$ psia. Within 0.2 s of becoming quiet, the flow on the nozzle wall separated until reattaching about one to three seconds later at $36 > p_t > 30$ psia. The finish of the electroformed nozzle within one inch of the bleed lip was degraded by the remachining (Figure 5.3). In June 2006 the nozzle was taken to Optek to restore the mirror-quality finish.
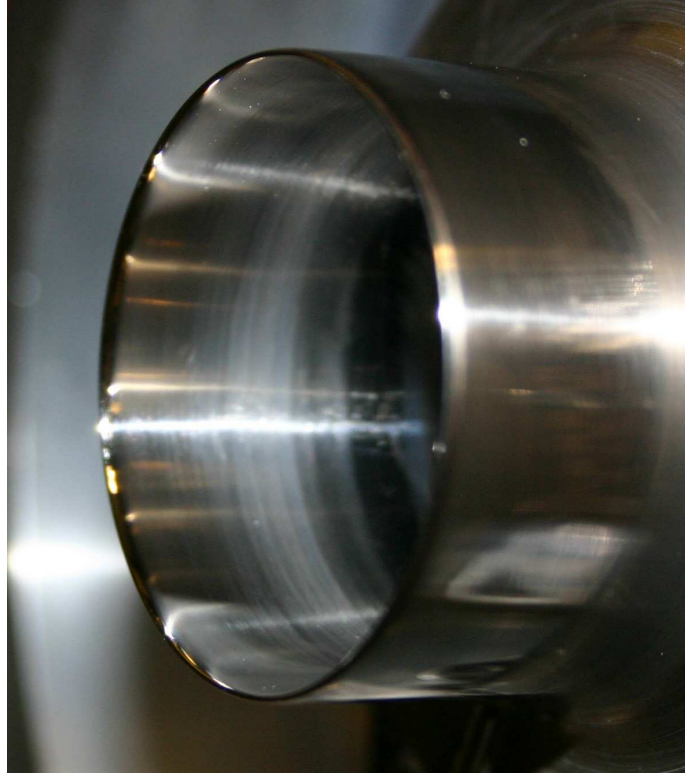
Figure 5.3: Remachined electroformed nozzle bleed lip; note poor surface finish

While the electroformed nozzle was being polished, the surrogate nozzle was used. It consistently ran quiet for $p_t < 94$ psia (up from 73 psia), even though no modifications had been made.

When the electroformed nozzle was returned from the polisher in July 2006, it was installed and inspected carefully. There were no visible scratches and the area near the remachined bleed lip was as highly-polished as the rest of the electroformed nozzle. The first tests showed a maximum quiet pressure of $p_t = 61$ psia. The nozzle was cooled and opened. The nozzle was still extremely clean, so no cleaning was necessary. The nozzle was reattached and reheated for about 20 hours. Tests revealed quiet performance up to $p_t = 91$ psia, which is very near the current performance of the surrogate nozzle. After two weeks of frequent operation into August 2006, the quiet pressure was still $p_t = 91$ psia.

The maximum quiet pressure of the electroformed nozzle was tested again in late August 2006. After one month of regular operation, the maximum quiet pressure had dropped slightly from 91 to 87 psia. The nozzle was cooled, detached, cleaned, reattached, reheated, and retested. The quiet pressure dropped to 77 psia. This process was repeated with a slight change in the reattachment procedure. Normally, after the alignment of the nozzle has been completed, Section 1 is bolted to the contraction without delay. This time, at first only two bolts were used, at a low torque, in order to keep Section 1 and the contraction in contact, allowing the nozzle to come to thermal equilibrium with the contraction before torqueing all bolts to specification. After one hour, the nozzle was warm and the normal procedure was resumed. The quiet pressure remained unchanged at 77 psia. The nozzle was opened and reattached once more. The usual reattachment procedure was used. The quiet pressure improved to 117 psia. This level of performance is near the highest achieved for the surrogate.

5.2   Itemized Account

A summary of experience is as follows:

Aft-Facing Step When the aft-facing step between Sections 4 and 5 was removed, the quiet pressure increased from 20 to 37 psia. There are no other such large steps to have removed. This modification was made before the variability between nozzle attachments was discovered. It is possible that this performance change is at least partly due to simply detaching and reattaching the nozzle.

Polish Unfortunately, the direct effect of the first polish was overshadowed by the nick in the bleed lip. The maximum quiet before the polish was 37 psia; afterward, it was 130 psia. The touch-up polish of the surrogate nozzle in May 2006 had no effect upon quiet pressure. In July 2006, improving the finish of the electroformed nozzle from machined to mirror-like achieved an increase in quiet pressure from 39 psia to 91 psia.

Nicked Bleed Lip The influence of the nick in the bleed lip cannot be precisely determined because it happened in conjunction with the polish. The maximum quiet pressure dropped from 37 psia to 12 psia with the nick. Subsequent repairs improved it to 34 psia, then 94 psia.

Misshapen Bleed Lip The electroformed nozzle has a better polish than the surrogate and no seams between sections, yet it was not quiet for $p_t > 8$ psia. The leading suspect was the 'kink' discovered in the electroformed bleed lip when measured by Anderson Tool & Engineering. The first tests of the remachined electroformed nozzle with the elliptical cross-section yielded quiet flow for $p_t < 39$ psia.

Separation Bubble on Bleed Lip Very small changes in the installation of the nozzle could modify the separation bubble enough to cause the erratic performance of the surrogate nozzle. Initial testing of the modified electroformed nozzle with the elliptical bleed lip indicated greater stability between installations, but this result may have been an effect of the poor finish. As of August 2006, the electroformed and surrogate nozzles have similar performance with similar polishes but different bleed lip profiles, suggesting that the separation bubble may not be critical, the bleed lip redesign has no effect, or that some other factor has become dominant.

Contraction Leaks Tests with leaks in the contraction only showed that the quiet pressure stayed above 122 psia. Even fairly large leaks did not drop the quiet pressure far.

Oil Streaks Along Nozzle Wall Streaks were first noted on the nozzle wall in January 2006. They were cleaned whenever the nozzle was opened. They returned twice, but to a lesser degree than before. Removing them had no clear effect on quiet pressure.

Accumulated Gunk After Section 1 In January 2006 an uneven step was noticed after Section 1. It turned out to be just some gunk and was removed in mid-February. After removal, the maximum quiet pressure actually decreased. The detrimental effect of the step must have been overshadowed by some other influence.

Temperature Equilibration Time During February 2006 the nozzle was opened for cleaning several times. After cleaning, it was reheated and tested within 24 hours. Though the contraction thermocouples showed that the temperature was nominal, there may have been nonuniformities. After another 60 hours of equilibration, the quiet pressure rose from 58 to 130 psia. The equilibration time could possibly be affecting a bleed lip-separation bubble. There are several counterexamples of constant quiet pressures as more time elapses after reheating the nozzle.

Dew Point The dew point of the air varied from -8 to -25 °C depending on time of year (drier during the winter) and time of day (wetter for the first run of the day). No effect of dew point was observed.

Seam at Joint between Sections 1 and 2 Even after the gunk was wiped away, a small step could be seen at the joint between Sections 1 and 2. It appeared to be an even step for all azimuths. The May 2006 polish removed the visible seam but did not improve performance.

Dust The maximum quiet pressure is frequently consistent from run to run, but it often has changed when the nozzle is detached and reattached, even if no changes were made. One possible explanation is dust in the nozzle. Care is taken to clean the nozzle before closing it. Also, there are some unexplained improvements in performance between runs that could be due to dust blowing out of the tunnel. Because the dust level before, during, and after a run cannot be measured, it is difficult to assess its effect.

6. Tunnel Uniformity & Consistency

6.1 Nozzle and Test Section Uniformity

Several tests were conducted with the surrogate nozzle to characterize the flow quality in the tunnel nozzle and test section. The quiet pressure and noise levels were consistent at various axial and radial locations.

6.1.1 Axial Independence of Quiet Pressure and Noise Level

Though most data were collected from a pitot near the end of the nozzle (1.93 m $< z <$ 2.37 m), on two occasions a far-forward pitot was mounted in the forward-bottom access port in Section 8. This pitot reached farther up the nozzle, to $z =$ 1.15 m.

Surrogate nozzle noise level data for two runs at the same start conditions with different pitot locations are shown in Figure 6.1. Transition to low noise levels occurs when $p_t \approx$ 95 psia, at both locations. A similar axial independence was noted earlier, before the first polish, when the tunnel was only quiet for $p_t \leq$ 37 psia (Figure 6.2).

These results suggest a bypass mechanism for the transition of the nozzle boundary layer. An axial dependence of quiet pressure, on the other hand, would have suggested nozzle-wall boundary-layer transition at differing axial locations, as in the classic NASA Langley studies.

6.1.2 Radial Symmetry of Quiet Pressure

The radial uniformity of quiet pressure and noise level was assessed in June 2006 with the surrogate nozzle, which was quiet for $p_t <$ 94 psia at the time. A pitot pressure transducer was located at $z =$ 2.16 m, which is forward of the traverse
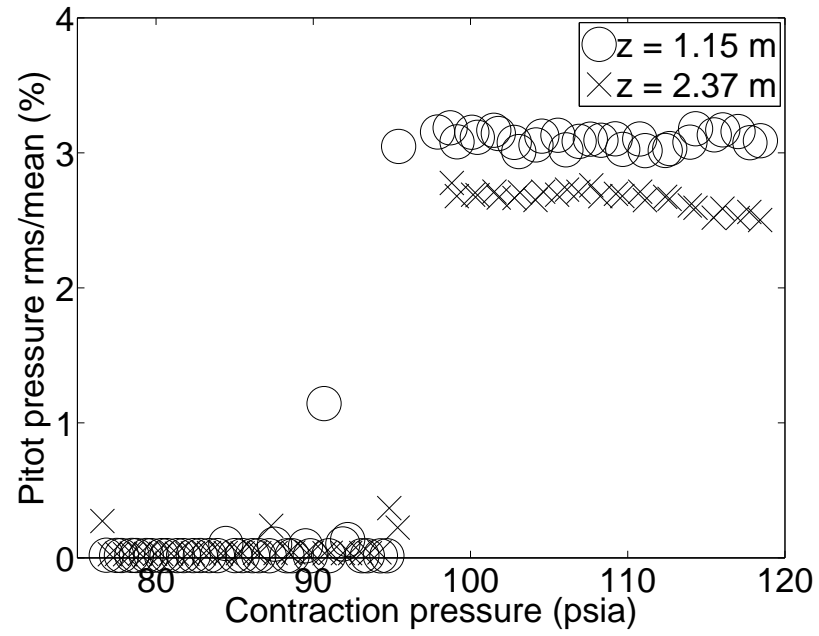
Figure 6.1: Axial independence of quiet pressure of $p_t = 95$
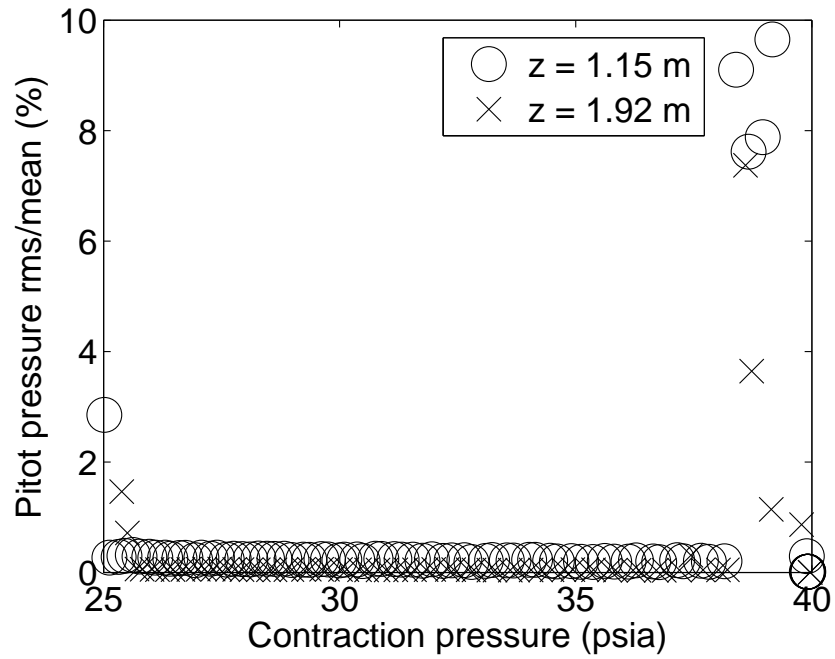
Figure 6.2: Axial independence of quiet pressure of $p_t = 37$

slot. Runs were conducted with the pitot probe along the centerline ($y = 0$), 3.0 cm above and below, and 9.0 cm above the centerline. Figure 6.3 illustrates that the flow became quiet at the same $p_t = 94$ psia for all radial locations. At $y = 9.0$ cm, which is 2.5 cm from the nozzle wall, the noisy portion of the run is much noisier than for the other locations, probably because of the close proximity of the turbulent boundary layer.
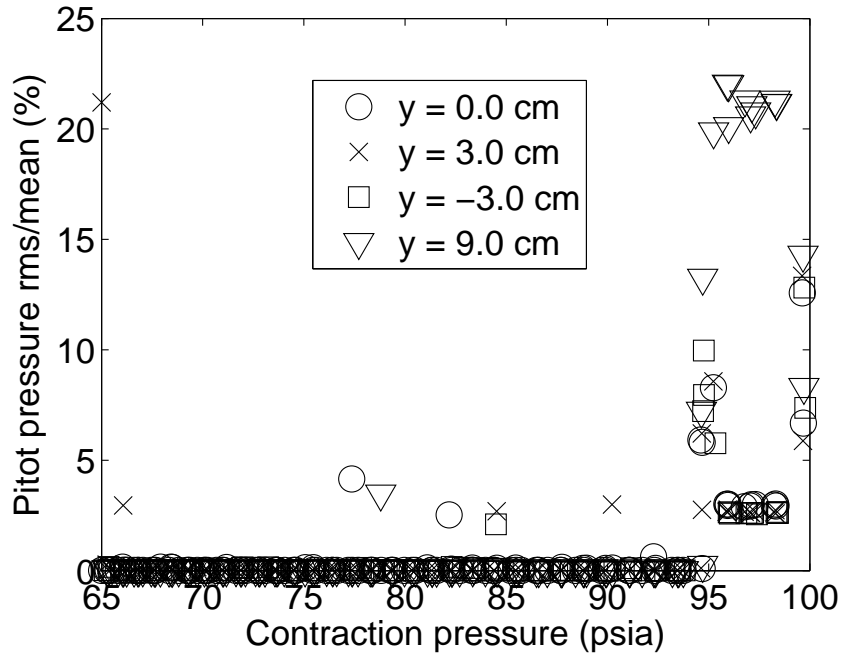
Figure 6.3: Radial dependence of quiet pressure

Figure 6.4 contains the same data as Figure 6.3, but is zoomed in on the quiet part of the run. For $94 > p_t > 85$ psia, the first 1.5 s of quiet flow, the flow near the nozzle wall is just as quiet as the flow elsewhere. After that time, the flow near the wall is less quiet ($0.04 < \tilde{p}/\bar{p} < 0.06\%$), but still near the quiet-flow criterion of $\tilde{p}/\bar{p} < 0.05\%$. The noise levels for the other locations increase slightly as well, more so for the off-center measurements. The handful of noise levels between 0.07 and 0.10% are the results of turbulent bursts.
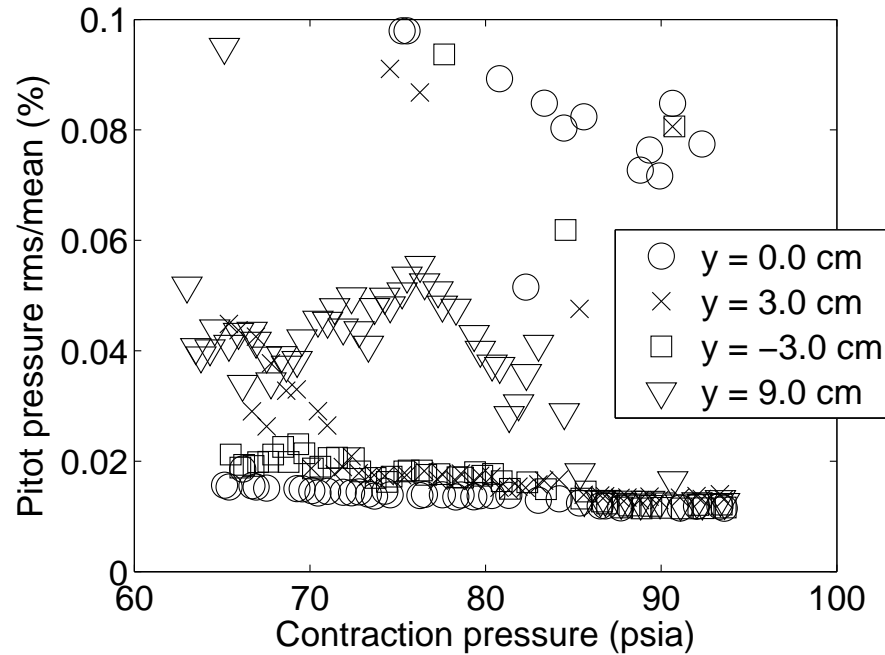
Figure 6.4: Radial dependence of quiet pressure (quiet portion)

This radial independence of quiet pressure, in conjunction with axial independence, demonstrate good uniformity of the flow properties throughout the test section.

6.2 Consistency of Tunnel Performance

6.2.1 Settling Time Dependence of Quiet Pressure and Noise Level

In January 2006, when the tunnel's maximum quiet pressure was greater than the maximum allowable working pressure of 122 psia, the settling time between filling and running the tunnel was varied. It was thought that a shorter settling time might reduce the quiet pressure enough that the switch from noisy to quiet flow could be observed during the run. Normally, one waits ten minutes between the conclusion of filling the driver tube and initiating the run. Sometimes the diaphragms burst early and the settling time is less than ten minutes; sometimes there is a delay for

the vacuum tank pressure to be low enough, and the settling time is greater than nominal. Another goal of these tests was to determine if those variations in procedure caused a variation in performance.

A third goal of these tests was to understand the unusual shape in the pitot AC pressure traces during this session in the tunnel (Figure 6.5). Though the entire runs were quiet (with the exception of turbulent spikes), the first two seconds of the run were quieter than the rest.
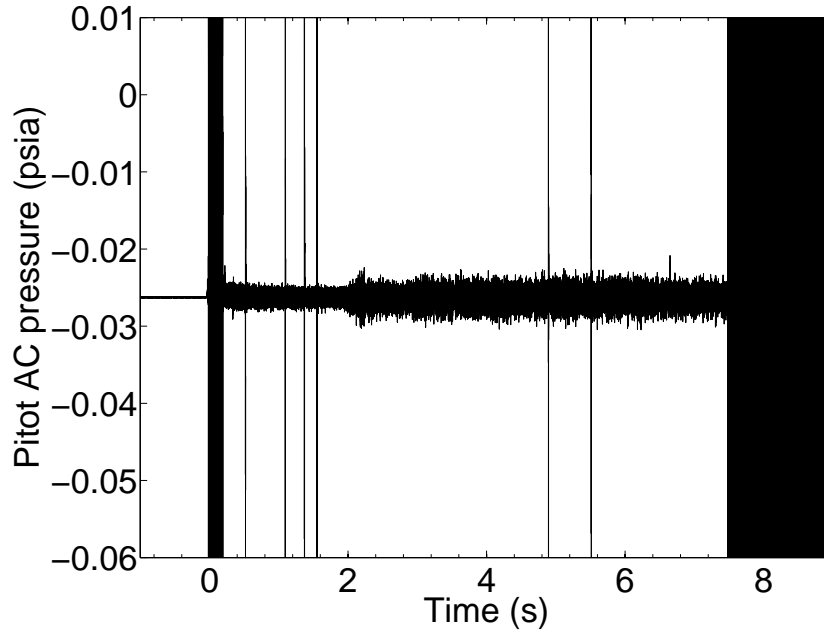
Figure 6.5: Pitot AC pressure with slight increase in noise at $t = 2.1$ s

Figure 6.6 contains a comparison of tunnel noise levels during the course of runs with different settling times. The baseline case is 10 minutes. These three runs were conducted over two days and the tunnel configuration was the same. For each case the run start pressure was 122 ± 0.5 psia and the run was quiet throughout. The noise level does not depend strongly upon the settling time. The increase in noise level occurs at the same contraction pressure (or time into the run) and has about the same magnitude. The only difference appears to be that the first two seconds of

the one-minute-settling-time case were less quiet than the others (though the noise level was still $< 0.025\%$).
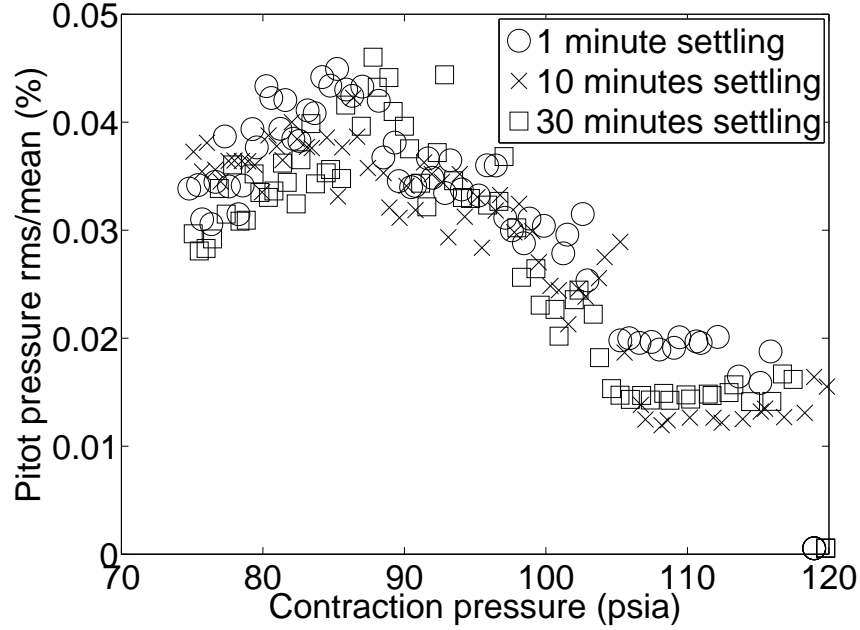
Figure 6.6: Noise level dependence on settling time

Even a very short, one-minute settling time did not leave the air in the driver tube so disturbed as to decrease the quiet pressure below 122 psia. Unfortunately, it is impossible to tell the effect precisely from these data because the runs were always entirely quiet. It does indicate that data from runs in which the diaphragms burst early may still have significant value and also that waiting any longer than the usual ten minutes does not achieve any benefit with regards to noise level. It is also apparent that the increase in noise level after 2 seconds did not depend on settling time. This phenomenon has not been explained and is still observed occasionally.

6.2.2 Effect of Jet into Upstream End of Driver Tube

Another attempt to lower the quiet pressure below the MAWP in January 2006 was to run the tunnel without turning off the pressure regulator and closing the

solenoid valve at the upstream end of the driver tube. Thus, the tunnel was still filling when the run began and throughout its duration. This test simulates an even earlier burst than the previous (one-minute settling time) test. The pressure regulator controller was set to 3.6 V, the typical final setting when filling to 120 psia. Once again, no change in the maximum quiet pressure was observed because it remained above the MAWP. The noise level versus contraction pressure exhibited the same behavior as other runs during this session in the tunnel. Initially there was lower noise, then an increase peaking near $p_t = 90$ psia, and then a decrease (Figure 6.7). Though the noise level was greater than the baseline case, it was still low.
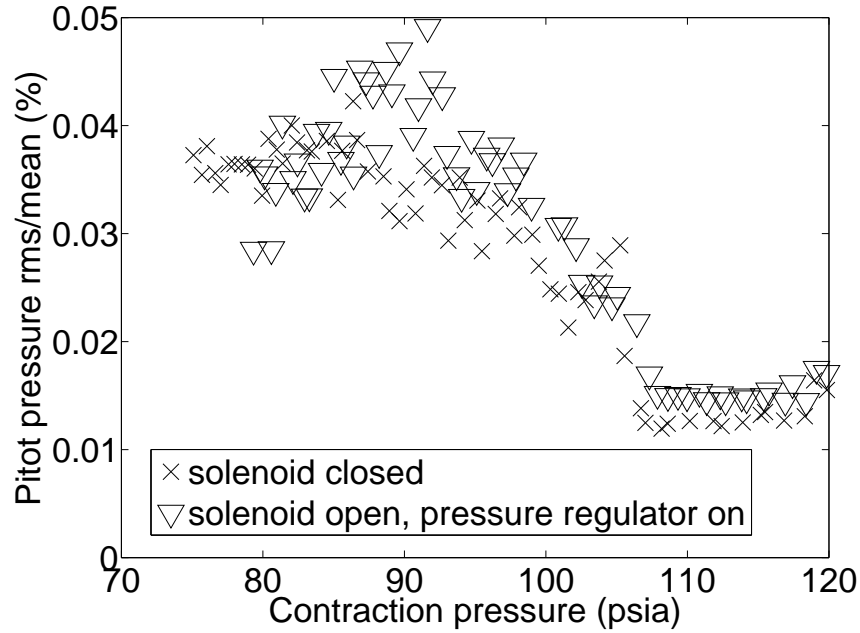
Figure 6.7: Effect of jet into upstream end of driver tube

6.2.3 Starting Pressure Dependence of Quiet Pressure

During September 2005, while the tunnel was quiet for $p_c < 94$ psia, several runs were conducted for identical test conditions except for different initial driver

tube pressures. To a limited degree, runs beginning at higher driver tube pressures tended to become quieter at higher pressures (Figure 6.8). However, starting pressures greater than 10% above the quiet pressure had no additional effect. Furthermore, there was no evidence that a slightly higher maximum quiet pressure could be obtained with a starting pressure very near the quiet pressure (so that the entire run is quiet).
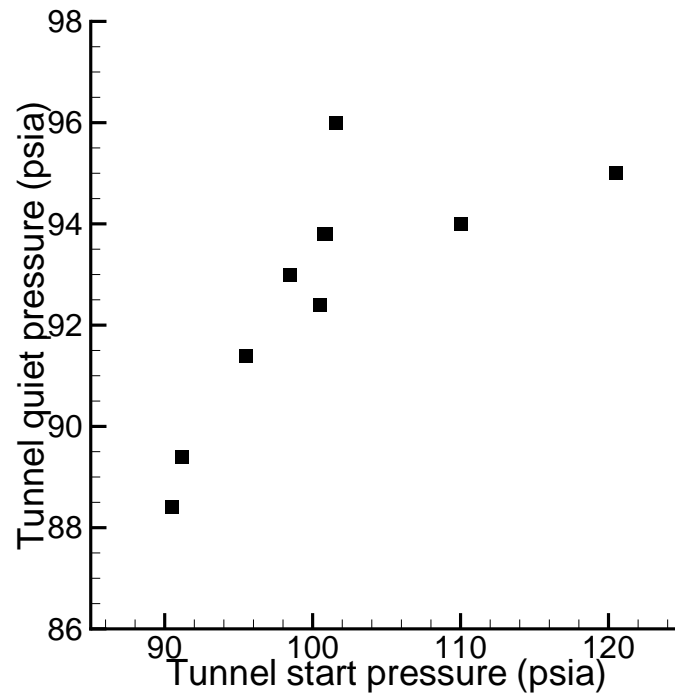
Figure 6.8: Quiet pressure dependence on start pressure

This weak sensitivity to starting pressure means that, for the purposes of consistent quiet pressures, one need not worry about precisely matching driver tube pressure from run to run.

6.3 Tunnel Blockage & Separation

Shocks emanating from a model in the test section or the model mount in the diffuser of a supersonic wind tunnel will interact with the boundary layer on the tunnel wall. Disturbances in supersonic flow can only travel downstream, but previous studies in the BAM6QT have shown that disturbances in the subsonic flow in the boundary layer can lead to separated flow upstream in the tunnel nozzle [29]. Laminar boundary layers are more likely to separate than turbulent ones [37], so shock/boundary layer interactions are more likely to affect upstream flow now that the tunnel runs with laminar boundary layers to higher Reynolds numbers.

In November 2005, a 4-inch-base-diameter 7° sharp cone was mounted in the tunnel at zero angle of attack with its tip at $z = 2.035$ m. A pitot pressure transducer was located at $z = 2.373$ m, 0.060 m above the center line. The uncalibrated hot-film array was employed for its ability to identify noisy, quiet, and separated flow in the boundary layer.

Figure 6.9 contains pitot pressure and hot-film voltage traces from a run beginning at $p_t = 90.4$ psia. At the time, the surrogate nozzle was quiet for $p_t < 94$ psia. This run is quiet from $t = 0$ s for about 0.6 s, at which point the nozzle-wall boundary layer separates. The separation is revealed by the increase in pitot pressure and hot-film voltage during $0.6 < t < 2.2$ s. After the flow reattaches, the noise level is low again.

Figure 6.10 is similar to Figure 6.9, except the run begins at $p_t = 104.9$ psia, above the maximum quiet pressure. The run begins noisy but becomes quiet when $p_t = 96$ psia. As soon as the nozzle-wall boundary layer becomes laminar, the flow separates. Unfortunately, the pitot DC pressure trace is off the oscilloscope scale during separation. As in the previous case, the flow reattached at $t \approx 2.5$ s and was quiet thereafter. The noisy, separated, and quiet flow as well as turbulent bursts are all visible in both the pitot and hot-film traces.
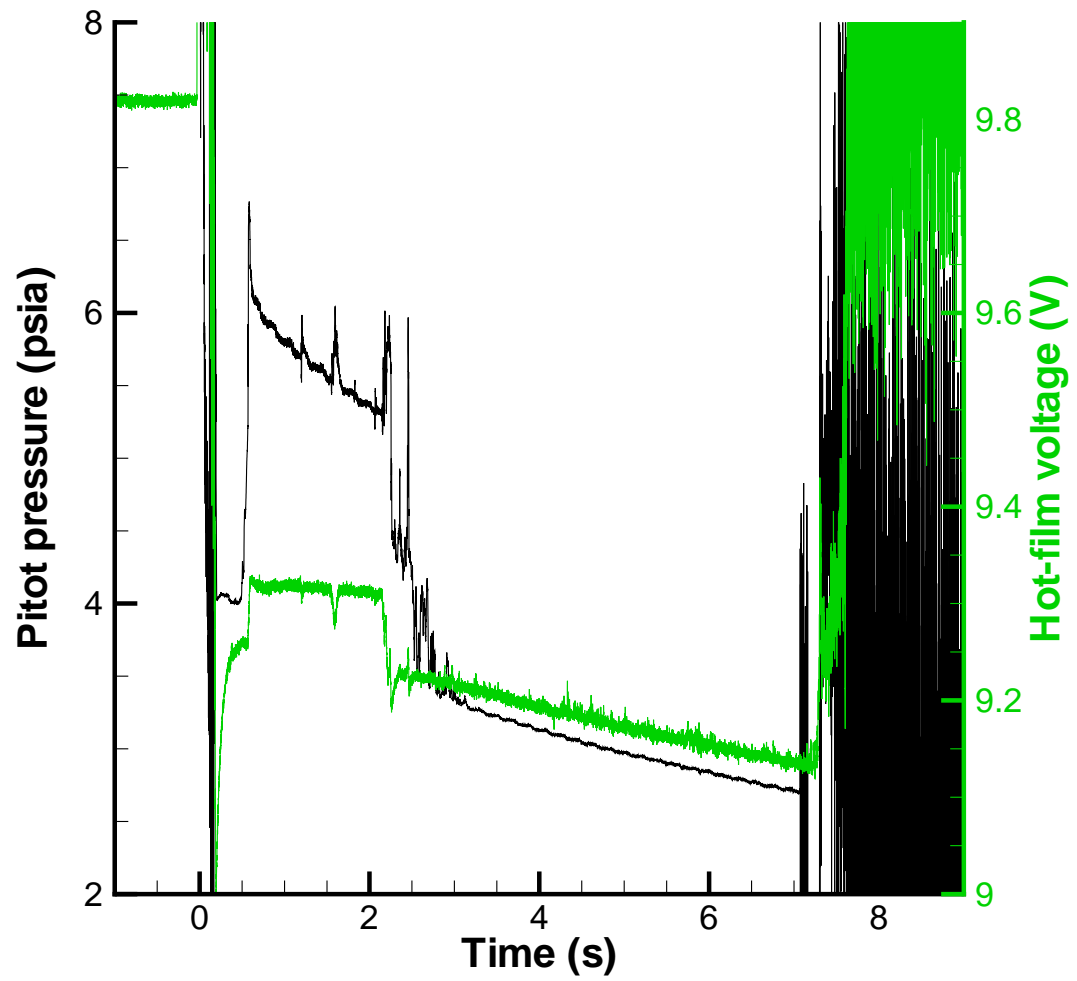
Figure 6.9: Nozzle-wall boundary-layer separation for run starting at $p_t = 90$ psia
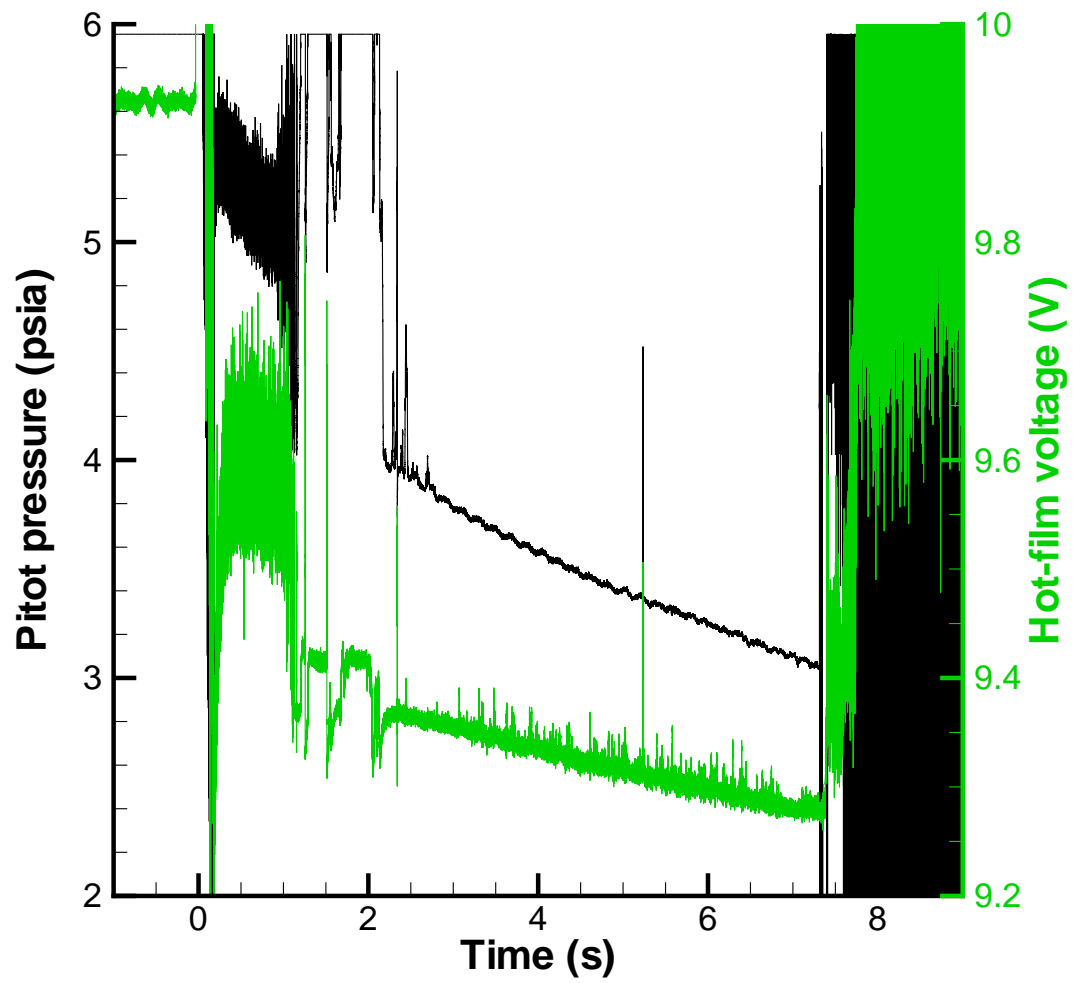
Figure 6.10: Nozzle-wall boundary-layer separation for run starting at $p_t = 105$ psia

One surprising feature of the flow in these cases is that the flow reattaches after the Reynolds number has decreased. Lower Reynolds numbers correspond to thicker boundary layers and greater risk of disturbances feeding forward. It would therefore be expected that a run would start noisy and attached, become quiet while remaining attached, and eventually separate for the rest of the run when the pressure drops too low. However, the trend of a larger separation region of laminar boundary layers agrees with experimental results for a compression ramp at Mach 6 presented in Reference [38] as well as the Free-Interaction Theory explained in Reference [39], which attributes the separation at higher Re to the lower skin friction. Unfortunately, the theory offers no explanation why separation does not occur for the present laminar boundary layers when $p_t > 50$ psia.

Shortly after the previous data were collected, the tunnel quiet pressure changed from $p_t = 94$ to 72 psia. This change occurred during a run. Two sets of noisy and quiet flow as well as separation are all visible in Figure 6.11. This run is only one to exhibit this behavior. For $0 < t < 3.5$ s, the run appears normal with some separation. (The separated pitot pressure is again cut off at the top.) The second half of the run, for $3.5 < t < 7$ s, also appears mostly normal, although the period of intermittent turbulence has distinct laminar portions. The peculiar switch from quiet to noisy flow is very abrupt.

After the above run, the tunnel remained quiet below $p_t = 73$ psia until the surrogate nozzle was swapped out. This subsequent repeatability is evidence against dust or other detritus flying through the tunnel and tripping the nozzle-wall boundary layer. Further runs with the cone model installed were conducted, but no separation was detected for this lower quiet pressure (Figure 6.12). The same tendency as in Figure 6.11 to have some laminar flow interspersed with intermittent turbulence is also present here.

Nozzle-wall boundary-layer separation was observed even without a model in the tunnel (but with the sting mount). Tests of the electroformed nozzle with newly-cut elliptical bleed lip exhibited quiet flow at $p_t = 39$ psia but separation within 0.2 s
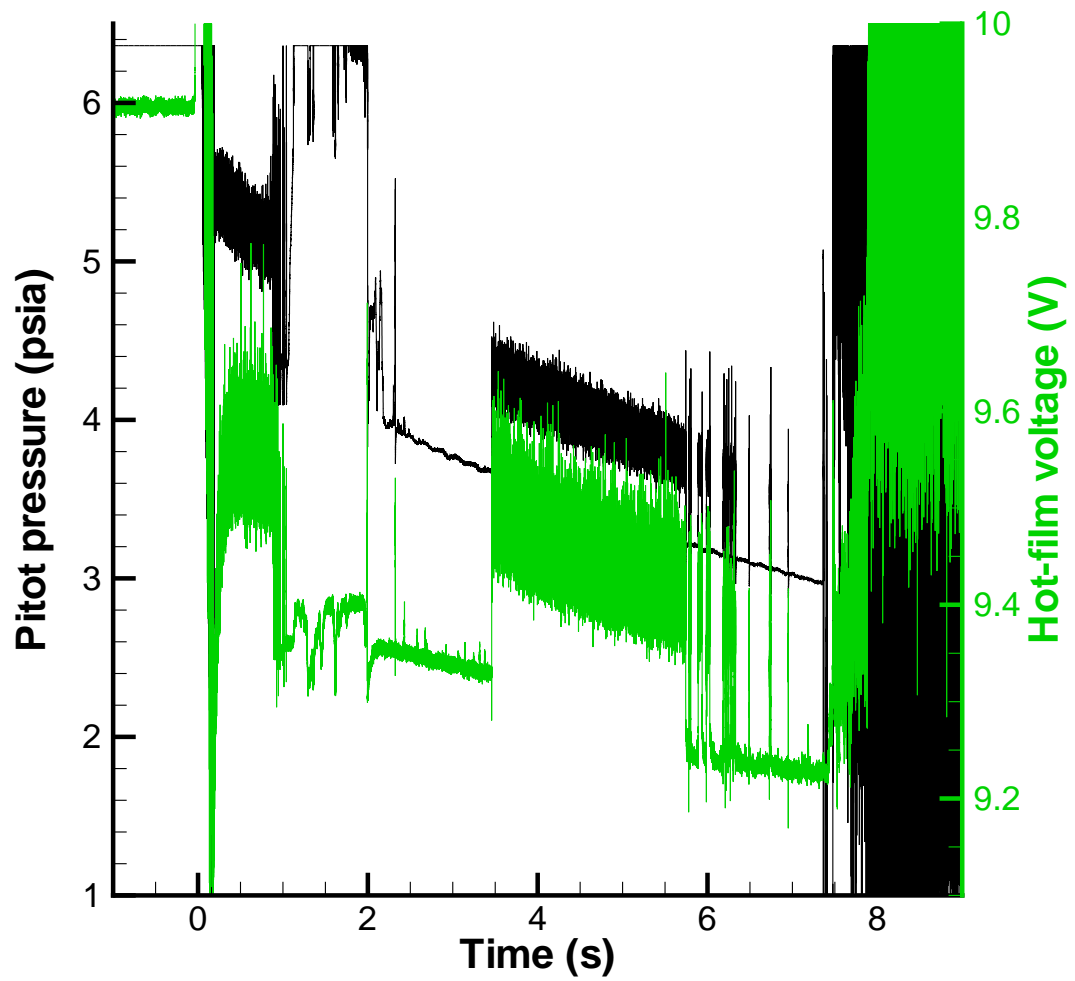
Figure 6.11: Nozzle-wall boundary-layer separation for run starting at $p_t = 106$ psia
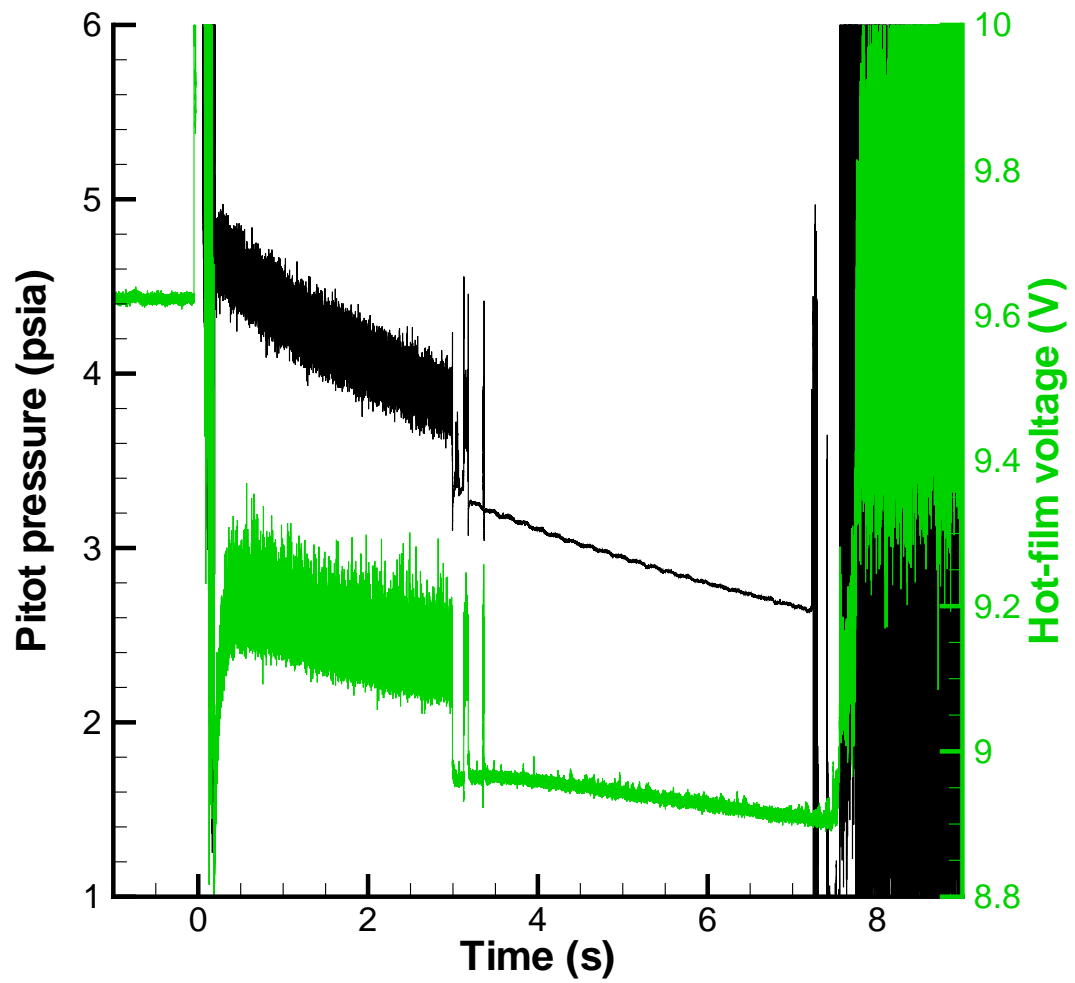
Figure 6.12: No separation for run starting at $p_t = 90$ psia

at $z = 2.37$ m downstream of the throat along the centerline (Figure 6.13). The test was repeated with the probe further upstream at $z = 2.14$ m and no separation was detected. Similar separation with the surrogate nozzle and no model has been detected at quiet pressures near 50 psia.
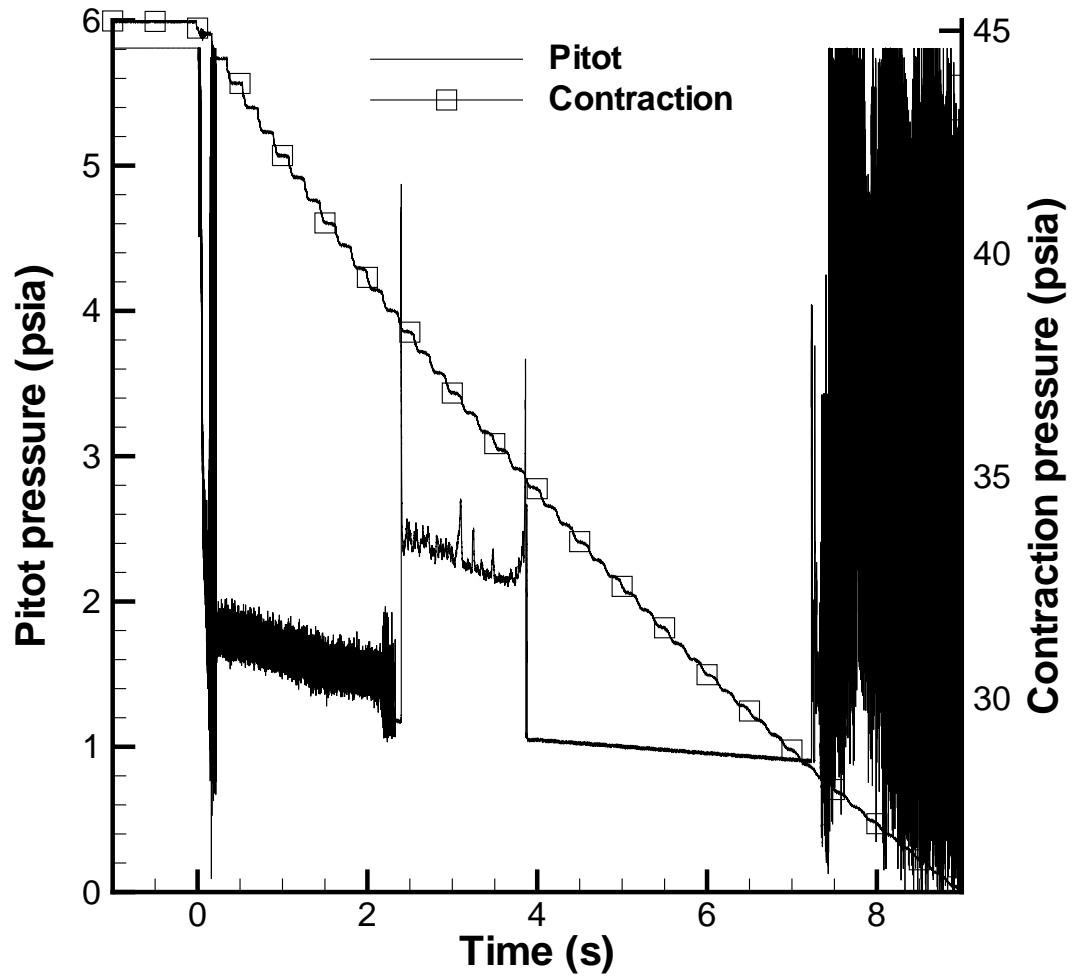
Figure 6.13: Separation with no model for run starting at $p_t = 45$ psia

7. Experimental Measurement of Sharp-Cone Flow

In November 2005, a 4-inch-base-diameter 7° sharp cone was mounted in the tunnel at zero angle of attack with its tip at $z = 2.035$ m in order to assess the effect of the model on nozzle-wall boundary-layer separation (see section 6.3). At this time, the tunnel was quiet for $p_t < 72$ psia. Figure 7.1 contains a pitot pressure trace for a run beginning at $p_t = 90$ psia. Rather than remaining stationary, the programmable traversing capability of the probe mount was employed to move the pitot pressure transducer through the oblique shock originating from the cone tip. In this run, the probe begins inside the shock and then moves away from the cone and outside the shock. It pauses for two seconds, during which p_t drops below 72 psia and the tunnel becomes quiet. The probe then descends back into the shock. The programmed angle between the probe and the cone centerline (ϕ) is the trapezoidal line on Figure 7.1, which refers to the right-hand axis.

The Mach number in the test section changes when the flow becomes laminar (see section 4.4), so the shock angle β changes. Whether the flow is noisy or quiet should not have any effect apart from the different Mach number in the test section. Figure 7.2 is a plot of the Mach number at the pitot probe. The probe is initially behind the shock, where $M = 5.26$. It exits the shock at $\phi = 13.1°$ and the Mach number increases to 5.70. While the probe is paused, the Mach number outside of the shock increases again, to 5.84, when the flow becomes laminar. The probe resumes its movement at $t = 4.37$ s and passes through the shock when $\phi = 12.7$ °.

The test was repeated for the same conditions except the pitot began outside of the shock, moved closer to the cone, and then returned upwards (Figures 7.3 and 7.4). The shock during the noisy portion of the run is encountered at $M = 5.66$ and $\phi = 13.0°$, and during the quiet portion, at $M = 5.79$ and $\phi = 12.8°$. The different Mach numbers between the runs account for the differences in shock angle.
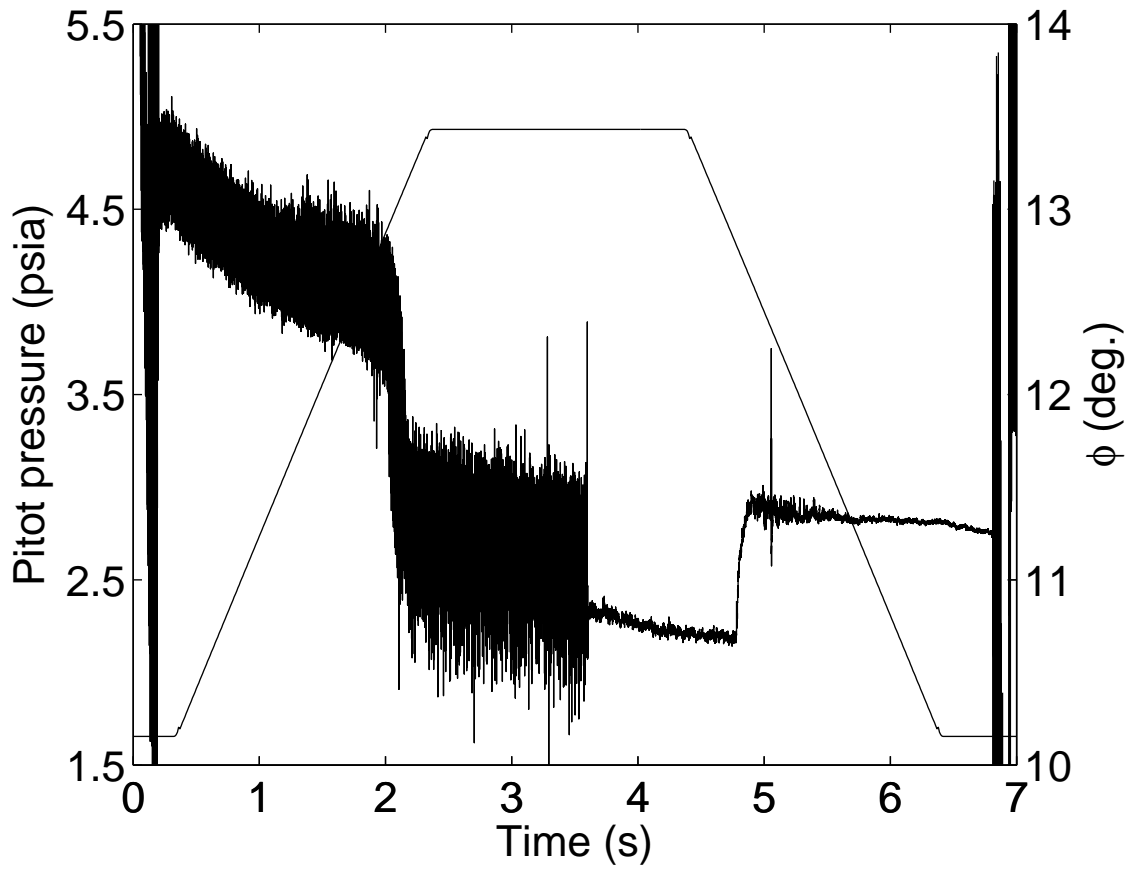
Figure 7.1: Pitot pressure as probe traverses out of and into conical shock
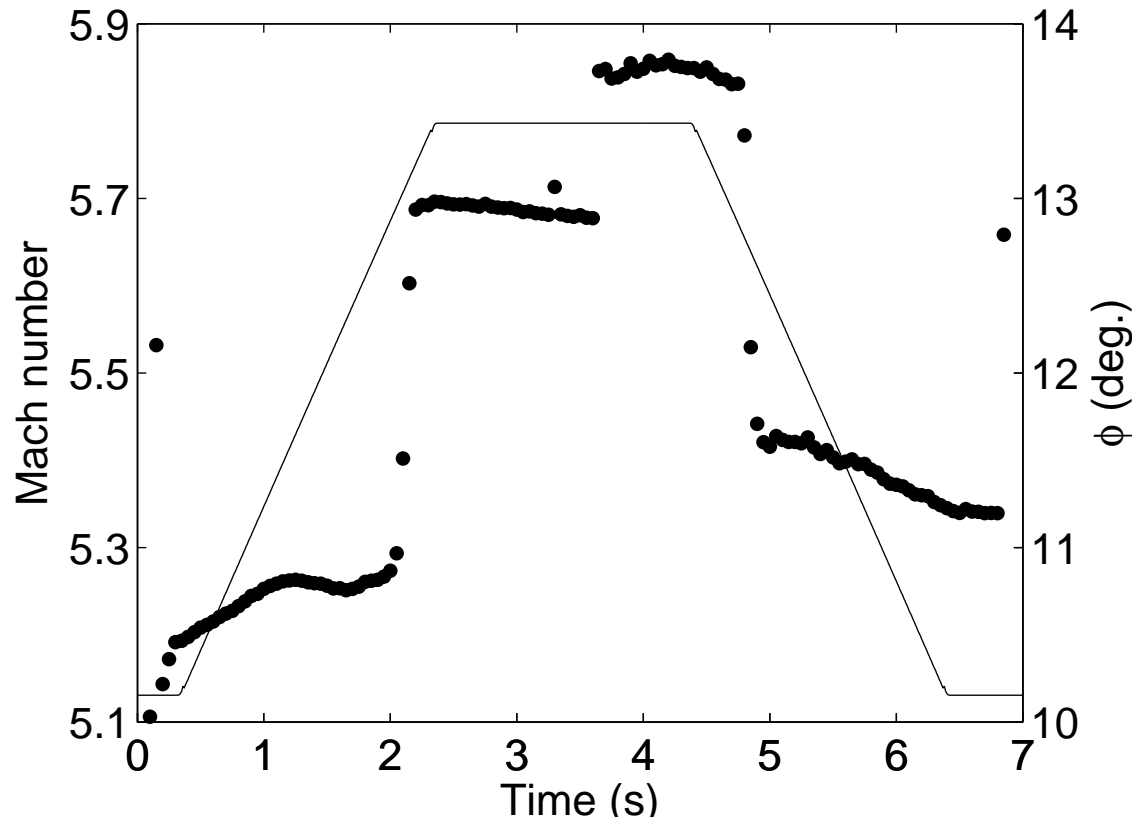
Figure 7.2: Mach number as probe traverses out of and into conical shock
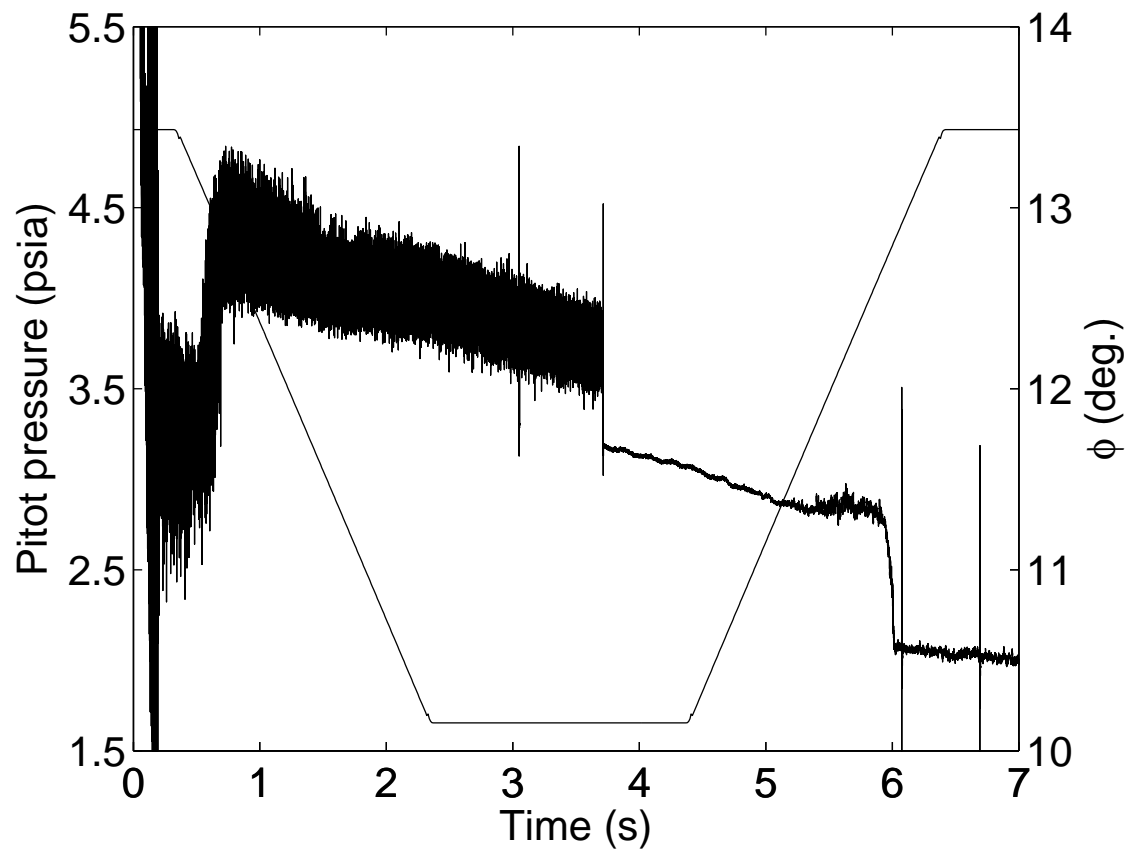
Figure 7.3: Pitot pressure as probe traverses into and out of conical shock
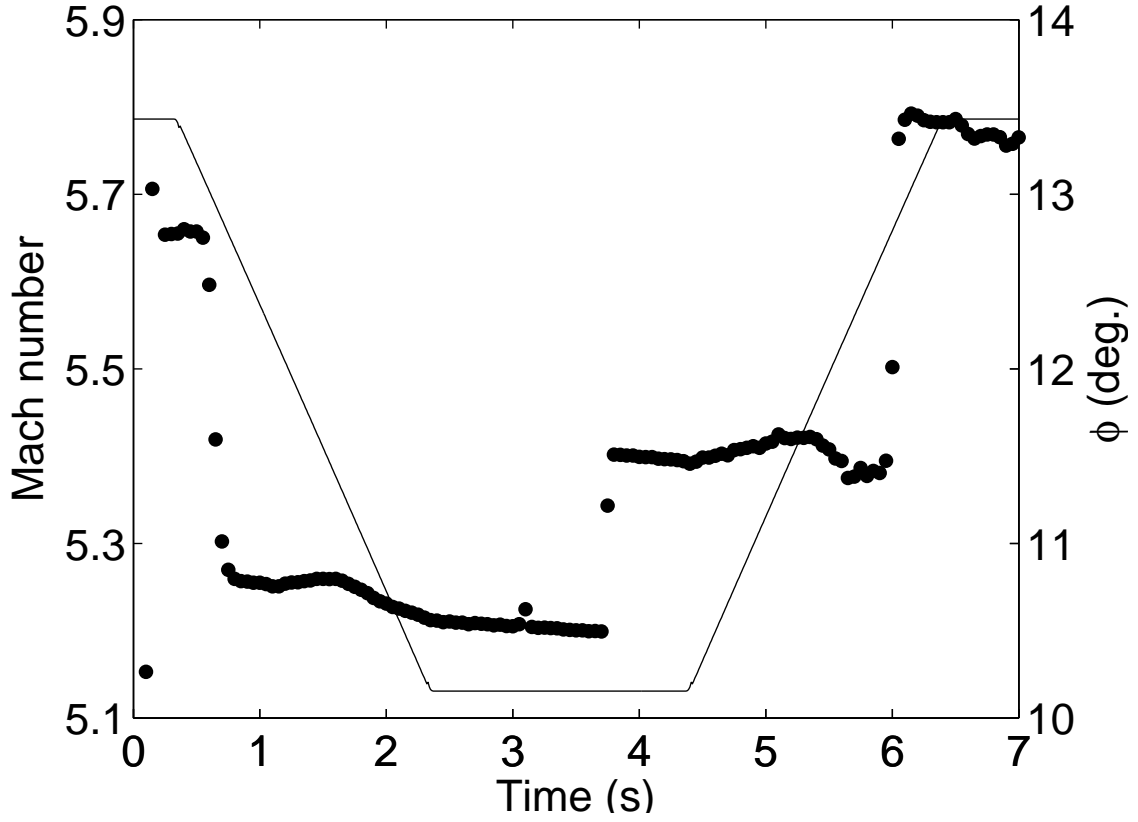
Figure 7.4: Mach number as probe traverses into and out of conical shock

A Fortran code from Reference [40] was employed to solve Taylor-Maccoll flow as a comparison to the experimental results. The code's inputs were the cone half angle, 7°, $\gamma = 1.4$, and $T_0 = 433$ K. The results are summarized in Table 7.1.

The computational results display the expected trends: β decreases and M_2 increases as M_1 increases. The experimental results follow the same trends except for β for $M_1 = 5.70$, which is larger than when $M_1 = 5.66$. The experimental Mach numbers and shock angles are all higher than those from the Taylor-Maccoll solution. This finding is curious because a larger shock angle should accompany a smaller Mach number. The percent errors between experimental and computational results are fairly small, 2.93–6.42%. An error of about 2 cm in the axial distance between

Table 7.1: Experimental & theoretical flow around a sharp cone

			Experimental			Taylor-Maccoll		% Difference	
Run	Condition	M_1	M_2	β (°)	M_2	β (°)	M_2	β	
2	Noisy	5.66	5.26	13.0	5.09	12.36	3.34	5.18	
1	Noisy	5.70	5.27	13.1	5.12	12.31	2.93	6.42	
2	Quiet	5.79	5.38	12.8	5.19	12.19	3.66	5.00	
1	Quiet	5.84	5.42	12.7	5.23	12.13	3.63	4.70	

the cone tip and pitot probe would account for the $\approx 0.6°$ difference between shock angles. However, the error in measuring this length is less than 5 mm. A 4 mm error in measuring the probe's radial location could also shift the shock location measurement by 0.6°, but the error in centering the pitot is less than 2 mm. A 2 mm error in the probe's radial location in conjunction with a 5 mm error in the probe's axial location creates a 0.5° difference — most of the observed error. A 2% error in the calibration of the pitot pressure transducer would only cause a $\approx 0.5\%$ change in Mach number. Taylor-Maccoll flow makes several assumptions: an attached shock on a perfectly-sharp cone, inviscid flow, an ideal gas, and constant c_p. A combination of imperfect assumptions, errors in axial and radial location measurements, and miscalibrated pressure transducers can account for the observed differences.

8. Conclusions and Future Work

The introduction of the surrogate nozzle led to a significant increase in the maximum quiet pressure of the BAM6QT, from 8 psia to more than 90 psia, although not reliably. As of August 2006, both the nickel electroformed and aluminum surrogate nozzles have similar maximum quiet pressures. This correspondence suggests that the bleed lip profile is not the limiting factor at this time. On the other hand, the removal of the nick from the electroformed nozzle bleed lip had a dramatic effect. The polish level of the nozzle also has a significant, though not definitive, effect on quiet pressure. There was a moderate performance increase when the remachined electroformed nozzle was polished. However, the mirror-like polish of the nickel performs no better than the very good polish of the aluminum.

Though this work has led to substantial improvements, two questions remain. The nozzle is designed for quiet performance for stagnation pressures up to 150 psia, 30% better than currently achieved. The bleed lip flaw and polish level have been identified as significant parameters, but there must be some other reason for the limited maximum quiet pressure.

The other unresolved issue is the reliability of the maximum quiet pressure. Levels as high as 130 psia have been obtained, and if the tunnel could run consistently at this high pressure the performance would be satisfactory. Tunnel performance changes substantially when the nozzle is detached and reattached. The reason for this sensitivity is not clear. A separation bubble on the bleed lip is still a candidate, but the recent tests with the elliptical bleed-lip profile have not been substantially better than the best results from the original bleed-lip profile. Further testing is needed with the new bleed lip to determine how reliably it performs.

LIST OF REFERENCES

LIST OF REFERENCES

[1] Eli Reshotko. Stability and transition, how much do we know? *U.S. National Congress of Applied Mechanics*, pages 421–434, June 1986. American Society of Mechanical Engineers.

[2] John D. Anderson Jr. *Hypersonic and High Temperature Gas Dynamics*, chapter 6, Viscous Flow: Basic Aspects, Boundary Layer Results, and Aerodynamic Heating. American Institute of Aeronautics and Astronautics, Inc., Reston, VA, 1989.

[3] Steven P. Schneider. Laminar-turbulent transition on reentry capsules and planetary probes. AIAA Paper 2005-4763, June 2005.

[4] Steven P. Schneider. Hypersonic laminar-turbulent transition on circular cones and scramjet forebodies. *Progress in Aerospace Sciences*, 40(1):1–50, February 2004.

[5] John Laufer. Aerodynamic noise in supersonic wind tunnels. *Journal of the Aerospace Sciences*, 28(9):685–692, September 1961.

[6] Ivan E. Beckwith. Development of a high Reynolds number quiet tunnel for transition research. *AIAA Journal*, 13(3):300–306, March 1975.

[7] S. R. Pate and C. J. Schueler. Radiated aerodynamic noise effects on boundary layer transition in supersonic and hypersonic wind tunnels. *AIAA Journal*, 7(3):450–457, March 1969.

[8] F.-J. Chen, M. R. Malik, and I. E. Beckwith. Boundary-layer transition on a cone and flat plate at Mach 3.5. *AIAA Journal*, 27(6):687–693, June 1989.

[9] Steven P. Schneider. Flight data for boundary-layer transition at hypersonic and supersonic speeds. *Journal of Spacecraft and Rockets*, 36(1):8–20, January-February 1999.

[10] I. E. Beckwith, W. D. Harvey, J. E. Harris, and B. B. Holley. Control of supersonic wind-tunnel noise by laminarization of nozzle-wall boundary layers. Technical Report TM X-2879, NASA Langley Research Center, Hampton, VA 23665, December 1973.

[11] W. D. Harvey, P. C. Stainback, J. B. Anders, and A. M. Cary. Nozzle wall boundary-layer transition and freestream disturbances at Mach 5. *AIAA Journal*, 13(3):307–314, March 1975.

[12] I. E. Beckwith and P. C. Stainback. Transition research and prospects for a Mach 3 to 7 quiet tunnel. Langley Working Paper No. 1064, July 1972.

[13] I. E. Beckwith and E. W. Martin. Propagation of settling chamber noise in supersonic wind tunnels. *Meeting of the Supersonic Tunnel Association*, March 1982.

[14] I. E. Beckwith, T. R. Creel Jr., F. J. Chen, and J. M. Kendall. Free stream noise and transition measurements in a Mach 3.5 pilot quiet tunnel. AIAA Paper 1983-0042, January 1983.

[15] I. E. Beckwith, F.-J. Chen, and M. R. Malik. Design and fabrication requirements for low-noise supersonic/hypersonic wind tunnels. AIAA Paper 1988-0143, January 1988.

[16] I. E. Beckwith, F.-J. Chen, and M. R. Malik. Transition research in the Mach 3.5 low-disturbance wind tunnel and comparisons of data with theory. SAE Technical Paper Series No. 892379, September 1989.

[17] I. E. Beckwith, F.-J. Chen, S. P. Wilkinson, M. R. Malik, and D. Tuttle. Design and operational features of low-disturbance wind tunnels at NASA Langley for Mach numbers from 3.5 to 18. AIAA Paper 1990-1391, June 1990.

[18] I. E. Beckwith and C. G. Miller III. Aerothermodynamics and transition in high-speed wind tunnels at NASA Langley. *Annual Review of Fluid Mechanics*, 22:419–439, 1990.

[19] Steven P. Schneider. Design and fabrication of a 9.5-inch Mach-6 quiet-flow Ludwieg tube. AIAA Paper 1998-2511, June 1998.

[20] B. H. Carmichael. Summary of past experience in natural laminar flow and experimental program for resilient leading edge. NASA Contractor Report 152276, May 1979.

[21] Craig R. Skoch. Final assembly and initial testing of the Purdue Mach-6 quiet-flow Ludwieg tube. Master's thesis, Purdue University School of Aeronautics & Astronautics, December 2001.

[22] S. P. Schneider and C. Skoch. Mean flow and noise measurements in the Purdue Mach-6 quiet-flow Ludwieg tube. AIAA Paper 2001-2778, June 2001.

[23] S. P. Schneider, S. Matsumura, S. Rufer, C. Skoch, and E. Swanson. Progress in the operation of the Boeing/AFOSR Mach-6 Quiet Tunnel. AIAA Paper 2002-3003, June 2002.

[24] S. P. Schneider, C. Skoch, S. Rufer, S. Matsumura, and E. Swanson. Transition research in the Boeing/AFOSR Mach-6 Quiet Tunnel. AIAA Paper 2002-0302, January 2002.

[25] S. P. Schneider, S. Matsumura, S. Rufer, C. Skoch, and E. Swanson. Hypersonic stability and transition experiments on blunt cones and a generic scramjet forebody. AIAA Paper 2003-1130, January 2003.

[26] S. P. Schneider, C. Skoch, S. Rufer, and E. Swanson. Hypersonic transition research in the Boeing/AFOSR Mach-6 Quiet Tunnel. AIAA Paper 2003-3450, June 2003.

[27] S. P. Schneider, C. Skoch, S. Rufer, E. Swanson, and M. P. Borg. Bypass transition on the nozzle wall of the Boeing/AFOSR Mach-6 Quiet Tunnel. AIAA Paper 2004-0250, January 2004.

[28] S. P. Schneider, C. Skoch, S. Rufer, E. Swanson, and M. P. Borg. Laminar-turbulent transition research in the Boeing/AFOSR Mach-6 Quiet Tunnel. AIAA Paper 2005-0888, January 2005.

[29] Craig R. Skoch. *Disturbances from Shock/Boundary-Layer Interactions Affecting Upstream Hypersonic Flow.* PhD thesis, Purdue University School of Aeronautics & Astronautics, December 2005.

[30] Erick O. Swanson. Mean flow measurements and cone flow visualization at Mach 6. Master's thesis, Purdue University School of Aeronautics & Astronautics, December 2002.

[31] Selin Aradag. Purdue wind tunnel computational design report 1. Rutgers University unpublished report, January 2005.

[32] E. S. Taskinoglu and D. D. Knight. Computational fluid dynamics evaluation of bleed slot of Purdue Mach 6 Quiet Tunnel. *AIAA Journal*, 44(6):1360–1362, June 2006.

[33] S. Aradag and D. D. Knight. Computational design of the Boeing/AFOSR Mach 6 wind tunnel. AIAA Paper 2006-1434, January 2006.

[34] M. P. Borg, S. P. Schneider, and T. J. Juliano. Inlet measurements and quiet flow improvements in the Boeing/AFOSR Mach-6 Quiet Tunnel. AIAA Paper 2006-1317, January 2006.

[35] S. P. Schneider, T. J. Juliano, and M. P. Borg. High-Reynolds-number laminar flow in the Mach-6 quiet-flow Ludwieg tube. AIAA Paper 2006-3056, June 2006.

[36] R. H. Sabersky, A. J. Acosta, E. G. Hauptmann, and E. M. Gates. *Fluid Flow: A First Course in Fluid Mechanics*, chapter 8, Flow over External Surfaces. Prentice-Hall, Upper Saddle River, NJ, 1999.

[37] John D. Anderson Jr. *Fundamentals of Aerodynamics*, chapter 15.2, Qualitative Aspects of Viscous Flow. McGraw-Hill, New York, 3rd edition, 2001.

[38] J. E. Lewis, T. Kubota, and L. Lees. Experimental investigation of supersonic laminar, two-dimensional boundary layer separation in a compression corner with and without cooling. AIAA Paper 1967-191, January 1967.

[39] J. Delery and J. G. Marvin. Shock-wave boundary layer interactions. *AGARDograph No. 280*, 1986.

[40] Maurice J. Zucrow and Joe D. Hoffman. *Gas Dynamics: Volume II, Multidimensional Flow*, chapter 16-5, Taylor-Maccoll Flow Around a Cone. Robert E. Krieger Publishing Company, Inc., Malabar, FL, 2nd edition, 1985.

APPENDIX

A. Matlab Codes

A.1   Noise Level Calculation

This code was used to analyze the oscilloscope output and calculate noise level, Mach number, etc. Input is three or four oscilloscope files: pitot DC voltage, pitot AC voltage, and contraction voltage; plus, optionally, the hot-film output.

```
clear variables
tic;
date = '2006-7-20';
run = '1';


addpath(['..\data\',date,'\',run])
[vac,t]=tekread('ptac.wfm');
[vdc,t]=tekread('ptdc.wfm');
[vctdc,t]=tekread('ctdc.wfm');
% [hf,t2]=tekread('hf1.wfm');
toc;


% calibrations from 20 July 2006
% calibration of contraction pitot:
pctdc = (vctdc + 0.106459) / 0.042579;


% calibration of long/short traverse pitot:
pac = vac / 0.570095 / 100;
pdc = (vdc - 0.190585) / 0.570095;
```

```
length_of_record = 10; % s

sampling_freq = length(vac) / length_of_record; % Hz

points = 100;

perpoint = sampling_freq * length_of_record / points;

prms = zeros(points,perpoint);

pmean = zeros(points,1);

trms = zeros(points,1);

pct = zeros(points,1);

for n = 1:1:points

    prms(n,:) = pac(((n-1)*perpoint + 1):n*perpoint)';

    if max(prms(n,1:1000)) - pac(1) > 0.1 * (max(pac) - min(pac))

        prms(n,:) = pdc(((n-1)*perpoint + 1):n*perpoint)';

    end%if

    trms(n) = t(perpoint*n);

    rms(n) = sqrt(mean((prms(n,:) - mean(prms(n,:))).^2));

    pmean(n) = mean(pdc(((n-1)*perpoint + 1):n*perpoint));

    turb(n) = rms(n) / pmean(n) * 100;

    pct(n) = mean(pctdc(((n-1)*perpoint + 1):n*perpoint));

    p01 = pct(n);

    p02 = pmean(n);

    M(n) = Rayleigh_pitot(p01, p02, 0, 10);

end%for


toc;

fontsize = 16;

markersize = 16;


figure(1)

fig1 = plot(pct, turb, 'kx');
```

```
set(xlabel('Contraction pressure (psia)'),'fontsize',fontsize)

set(ylabel('Pitot pressure rms/mean (%)'),'fontsize',fontsize)

set(fig1, 'markersize', markersize)

set(gca,'fontsize', fontsize)


figure(2)

fig2 = plot(pct, M, 'kx');

set(xlabel('Contraction pressure (psia)'),'fontsize',fontsize)

set(ylabel('Mach number'),'fontsize',fontsize)

set(fig2, 'markersize', markersize)

set(gca,'fontsize', fontsize)


figure(3)

[AX,H1,H2] = plotyy(t, pdc, t, pctdc, 'plot');

set(xlabel('Time (s)'),'fontsize',fontsize)

set(get(AX(1),'Ylabel'),'String','Pitot pressure (psia)',...

    'fontsize',fontsize,'Color','k')

set(get(AX(2),'Ylabel'),'String','Contraction pressure (psia)',...

    'fontsize',fontsize,'Color','b')

set(AX(1),'fontsize', fontsize,'ycolor','k','XLim',[-1,9])

set(AX(2),'fontsize', fontsize,'ycolor','b','XLim',[-1,9])

set(H1,'Color','k')

set(H2,'Color','b')


figure(4)

fig4 = plot(t2, hf, 'k');

set(xlabel('Time (s)'),'fontsize',fontsize)

set(ylabel('Uncalibrated hotfilm voltage'),'fontsize',fontsize)

set(fig4, 'markersize', markersize)
```

```
set(gca,'fontsize', fontsize)


figure(5)
fig5 = plot(t, M, 'k');
set(xlabel('Time (s)'),'fontsize',fontsize)
set(ylabel('Mach number'),'fontsize',fontsize)
set(fig5, 'markersize', markersize)
set(gca,'fontsize', fontsize)


figure(6)
fig6 = plot(t, pac, 'k');
set(xlabel('Time (s)'),'fontsize',fontsize)
set(ylabel('Pitot AC pressure (psia)'),'fontsize',fontsize)
set(gca,'fontsize', fontsize)
toc;
```

A.2 Mach Calculation

This function solves the Rayleigh pitot function recursively. It employs the bi-sector method. It is a helper function for the above noise level calculation.

```
function [M] = Rayleigh_pitot(p01, p02, Mlow, Mhigh);
gamma=1.4;
M = (Mhigh + Mlow)/2;
p02overp1 = ( (gamma+1)^2*M^2 / (4*gamma*M^2-2*(gamma-1)) )^...
    (gamma/(gamma-1)) * (1-gamma+2*gamma*M^2) / (gamma+1);
p01overp1 = (1+(gamma-1)/2*M^2)^(gamma/(gamma-1));
p02overp01 = p02overp1/p01overp1;


if p02overp01 / (p02/p01) < 0.9999
```

```
        [M] = Rayleigh_pitot(p01, p02, Mlow, M);
elseif p02overp01 / (p02/p01) > 1.0001
        [M] = Rayleigh_pitot(p01, p02, M, Mhigh);
end%if
```

B. Figure Source Data

Table B.1 identifies which tunnel runs were used to create the figures presented herein.

Table B.1: Figure source data

Figure	Year	Month	Day	Run No.	Note
4.1	2005	Sep	27	15	
4.2	2005	Sep	27	15	
4.3	2005	Sep	27	15	
4.7	2005	May	26	21	
4.4	2005	Sep	27	15	
4.5	2005	Sep	27	15	
4.6	2005	Sep	27	15	
6.1	2005	Sep	27	16	$z = 1.15$ m
6.1	2005	Sep	27	15	$z = 2.37$ m
6.2	2005	Jun	27	16	$z = 1.15$ m
6.2	2005	Jul	4	5	$z = 1.92$ m
6.3	2006	Jun	26	6	$y = 0$ cm
6.3	2006	Jun	26	7	$y = 3.0$ cm
6.3	2006	Jun	26	8	$y = -3.0$ cm
6.3	2006	Jun	26	9	$y = 9.0$ cm
6.5	2006	Jan	27	7	
6.6	2006	Jan	27	17	1 minute
6.6	2006	Jan	27	7	10 minutes
6.6	2006	Jan	27	18	30 minutes

Continued on next page

Figure	Year	Month	Day	Run No.	Note
6.7	2006	Jan	27	7	closed
6.7	2006	Jan	27	19	open
6.9	2005	Nov	4	3	
6.9	2005	Nov	4	2	
6.11	2005	Nov	4	4	
6.12	2005	Nov	4	7	
6.13	2006	May	26	21	
7.1	2005	Nov	4	9	
7.2	2005	Nov	4	9	
7.3	2005	Nov	4	10	
7.4	2005	Nov	4	10	